Article

Developmental Cell

PAF-Myc-Controlled Cell Stemness Is Required for Intestinal Regeneration and Tumorigenesis

Graphical Abstract

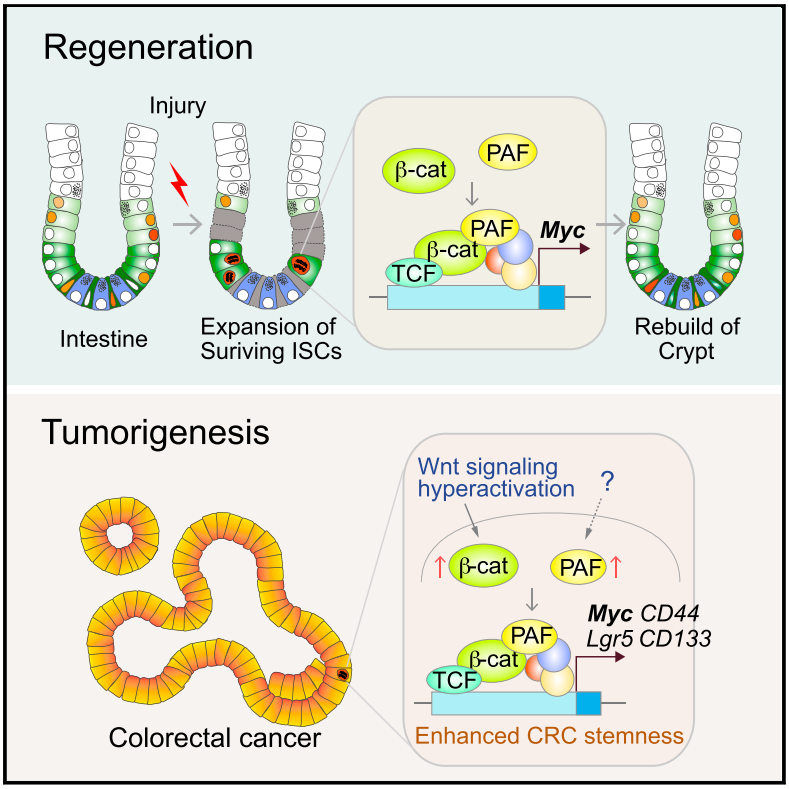

Highlights

- PAF is expressed in intestinal stem cells and upregulated in regenerating crypts
- PAF transactivates *c-Myc* in intestinal stem cells of the regenerating crypts
- PAF-Myc axis is required for intestinal regeneration
- PAF-Myc axis is required for stemness of colorectal cancer cells

Authors

Moon Jong Kim, Bo Xia, Han Na Suh, ..., Jie Zhang, Kaifu Chen, Jae-Il Park

Correspondence

jaeil@mdanderson.org

In Brief

Controlling the proliferation of self-renewing cells is crucial for tissue homeostasis and regeneration. Kim et al. show that PAF (PCNA-associated factor), dispensable for intestinal homeostasis, is required to positively regulate the proliferation of self-renewing cells via *Myc* transactivation during intestinal regeneration and tumorigenesis.

Kim et al., 2018, Developmental Cell *44*, 582–596
March 12, 2018
https://doi.org/10.1016/j.devcel.2018.02.010

CellPress

CellPress

Developmental Cell
Article

PAF-Myc-Controlled Cell Stemness Is Required for Intestinal Regeneration and Tumorigenesis

Moon Jong Kim,[1] Bo Xia,[2,3] Han Na Suh,[1] Sung Ho Lee,[1] Sohee Jun,[1] Esther M. Lien,[1] Jie Zhang,[1] Kaifu Chen,[2,3] and Jae-Il Park[1,4,5,6,*]

[1]Department of Experimental Radiation Oncology, University of Texas MD Anderson Cancer Center, Houston, TX 77030, USA
[2]Center for Cardiovascular Regeneration, Houston Methodist Hospital Research Institute, Houston, TX, USA
[3]Department of Cardiothoracic Surgery, Weill Cornell Medical College, Cornell University, New York, NY, USA
[4]Graduate School of Biomedical Sciences, University of Texas MD Anderson Cancer Center and Health Science Center, Houston, TX 77030, USA
[5]Program in Genetics and Epigenetics, University of Texas MD Anderson Cancer Center, Houston, TX 77030, USA
[6]Lead Contact
*Correspondence: jaeil@mdanderson.org
https://doi.org/10.1016/j.devcel.2018.02.010

SUMMARY

The underlying mechanisms of how self-renewing cells are controlled in regenerating tissues and cancer remain ambiguous. PCNA-associated factor (PAF) modulates DNA repair via PCNA. Also, PAF hyperactivates Wnt/β-catenin signaling independently of PCNA interaction. We found that PAF is expressed in intestinal stem and progenitor cells (ISCs and IPCs) and markedly upregulated during intestinal regeneration and tumorigenesis. Whereas PAF is dispensable for intestinal homeostasis, upon radiation injury, genetic ablation of *PAF* impairs intestinal regeneration along with the severe loss of ISCs and Myc expression. Mechanistically, PAF conditionally occupies and transactivates the *c-Myc* promoter, which induces the expansion of ISCs/IPCs during intestinal regeneration. In mouse models, *PAF* knockout inhibits *Apc* inactivation-driven intestinal tumorigenesis with reduced tumor cell stemness and suppressed Wnt/β-catenin signaling activity, supported by transcriptome profiling. Collectively, our results unveil that the PAF-Myc signaling axis is indispensable for intestinal regeneration and tumorigenesis by positively regulating self-renewing cells.

INTRODUCTION

Stem cells play key roles in tissue homeostasis and regeneration by self-renewing and repopulating progenitor cells (Fuchs et al., 2004; Morrison and Spradling, 2008). In the small intestine, two major intestinal stem cells (ISCs) co-exist. Crypt base columnar cell (CBC) ISCs marked by the high Lgr5 expression are highly proliferative and essential for the intestinal homeostasis (Barker et al., 2007). The other ISCs located at position 4 (+4) and labeled by Hopx, Lrig1, Bmi1, and Tert are quiescent during intestinal homeostasis, whereas they are conditionally activated upon tissue damage (Montgomery et al., 2011; Powell et al., 2012; Sangiorgi and Capecchi, 2008; Takeda et al., 2011). Accumulating evidence suggests that +4 ISCs function as a reservoir of ISCs during regeneration (Buczacki et al., 2013; Tian et al., 2011). In addition, the committed progenitor cells (Dll1+, Alpi+, and Krt19+) located above the position +4 cells also dedifferentiate into ISCs for intestinal regeneration (Asfaha et al., 2015; Tetteh et al., 2016; Van Es et al., 2012), implying the involvement of the cell plasticity in rebuilding intestinal epithelium. Although the extensive lineage tracing studies have been used to identify ISCs or reservoir ISC/intestinal progenitor cell (IPC) populations, still the underlying mechanisms of how these ISCs/IPCs are activated and expanded during regeneration remain elusive.

It was proposed that cancer stem cells (CSCs) are a subpopulation of tumor cells, which drives tumor growth by self-renewing and giving rise to the daughter cells (Nguyen et al., 2012). The identities of CSCs are still controversial, however, it is plausible that CSCs might be related to therapeutic resistance and tumor recurrence (Dean et al., 2005; Kreso and Dick, 2014). Expression of CD44, CD133, and Lgr5 have been suggested as a maker for stemness of colorectal cancer cells (CRCs) (O'Brien et al., 2007; Ricci-Vitiani et al., 2007; Schepers et al., 2012; Zeilstra et al., 2008; Zhu et al., 2009). Nonetheless, how CSCs are maintained and expanded were not fully understood.

Proliferating cell nuclear antigen (PCNA)-associated factor (PAF, also known as *p15/KIAA0101/NS5ATP9/OEACT-1*) was initially identified as a PCNA-interacting protein (Yu et al., 2001). PAF is implicated in both DNA repair and cell proliferation (Emanuele et al., 2011; Povlsen et al., 2012). PAF binds to the PCNA sliding clamp and regulates DNA replication and repair (De Biasio et al., 2015). Importantly, *PAF* expression is significantly upregulated in many human cancers (Cheng et al., 2013; Hosokawa et al., 2007; Jain et al., 2011; Jung et al., 2013; Kais et al., 2011; Kato et al., 2012; Mizutani et al., 2005; Wang et al., 2016; Yu et al., 2001; Yuan et al., 2007). In pancreatic cancer cells, *PAF* overexpression is necessary for pancreatic cancer cell proliferation (Hosokawa et al., 2007). In addition, PAF is associated with MAPK hyperactivation via transcriptional activation of the late endosomal/lysosomal adaptor, MAPK, and mTOR activator 3 (*LAMTOR3*), which is involved in the initiation of pancreatic intraepithelial neoplasia (Jun et al., 2013). Moreover, PAF hyperactivates Wnt/β-catenin signaling in CRCs as a co-factor of the β-catenin/EZH2 transcriptional complex, resulting in the development of intestinal adenoma (Jung et al., 2013).

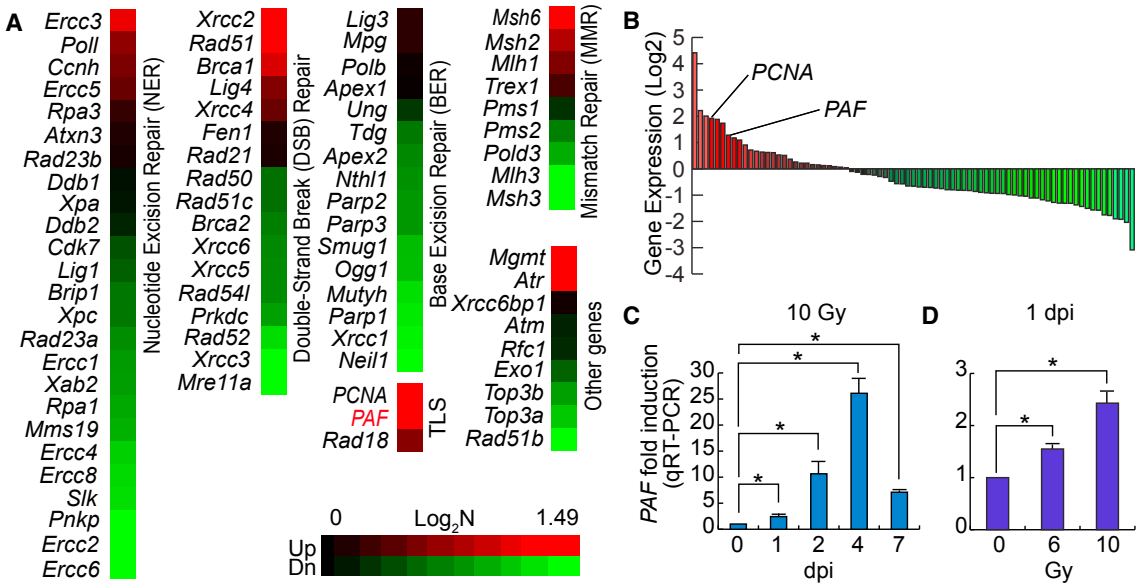

Figure 1. Upregulation of PAF Expression upon Radiation Injury

(A and B) Gene expression profiling of DNA repair genes upon radiation injury in mouse small intestine. After treatment of 10 Gy irradiation (1 day post-injury [1 dpi]), the whole small intestine samples were analyzed by qRT-PCR (n = 3). *PCNA* is the fourth and *PAF* are the seventh upregulated genes among the 79 genes related to DNA repair.

(C) Time-dependent upregulation of *PAF* expression upon IR injury. At 0, 1, 2, 4, and 7 dpi, the small intestine samples were collected and analyzed by qRT-PCR (n = 3).

(D) Dose-dependent upregulation of *PAF* expression upon injury. 6 and 10 Gy irradiation were used (1 dpi).

Student's t test; error bars = SEM; *p < 0.05.

In this study, we sought to interrogate how stem cells are activated by radiation injury. Our unbiased gene expression screening identified that, among DNA repair-related genes, *PAF* expression is associated with controlling ISCs/IPCs. Further comprehensive and genetic approaches revealed that the PAF-Myc signaling axis is indispensable for intestinal regeneration and tumorigenesis by positively controlling the expansion of stem cells.

RESULTS

Upregulation of *PAF* Expression upon Radiation Injury

To identify essential genes associated with DNA repair during tissue regeneration, we conducted a qRT-PCR array for DNA repair gene collections from irradiation (IR)-treated mouse small intestine (1 day post-injury [1 dpi], 10 Gy) (Figures 1A and 1B). Among 79 differentially expressed genes, *PAF* expression was highly upregulated by IR (ranked seventh). In addition, IR upregulated *PAF* expression in the mouse small intestine in a dose- and time-dependent manner (Figures 1C and 1D), which led us to hypothesize that PAF plays crucial roles in intestinal regeneration.

PAF Expression in Replenishing and Regenerating Intestinal Crypts

To elucidate the *in vivo* roles of PAF in intestinal regeneration, we generated a *PAF* knockout (KO) mouse model using a CRISPR/Cas9 gene targeting system (Wang et al., 2013; Yang et al., 2013) (Figure S1). Of note, *PAF* KO mice are viable without any discernible phenotypes. To examine PAF expression in the crypt, we conducted immunohistochemistry (IHC) using two different PAF monoclonal antibodies (Figures 2A and S2B). We confirmed the specificity of PAF antibody using *PAF* KO mice as a negative control (Figures 2A and S2B). We located five to ten cells of PAF positive (PAF+) cells in one section of crypt (Figures 2A and 2B). PAF was expressed in one to two cells of CBC ISCs and three to eight cells of transit-amplifying (TA) cells (Figures 2A and 2B), but not in the villi (Figure S2A). Most PAF+ cells belong to Ki67+ cells (17.71% of Ki67+ cells), a marker for cell proliferation (Figures 2C and 2E). Despite the additional role of PAF in DNA repair as a PCNA-interacting protein (Povlsen et al., 2012), only 23.01% of PAF+ cells were PCNA+ cells (Figures 2D and 2E). Furthermore, *PAF* KO mice did not display differences in the expression of *PCNA* in the crypts, compared with *PAF* wild-type (WT) mice (Figure 2F), implying the existence of PCNA-independent functions of PAF in the intestine.

To determine whether PAF is expressed in ISCs, we used a *Lgr5-EGFP-CreERT* knockin mouse. PAF+ cells were correlated with Lgr5+ CBCs and Lgr5+ progenitor cells localized at the TA zone (Figure 2H), confirmed by qRT-PCR of fluorescence-activated cell sorting (FACS)-isolated Lgr5+ cells (Figure 2I). The Paneth cells between CBC ISCs did not express PAF (Figure 2G). We further asked whether PAF is expressed in the quiescent ISCs at position 4, using *TERT-tdTomato-CreERT2* (Jun et al., 2016) and *Bmi1-EGFP* (Hosen et al., 2007) knockin mice. Some populations of TERT+ (52.94%) and Bmi1+ cells (63.16%) expressed PAF (Figures 2J, 2K, S2D, and S2E). These results indicate that PAF+ cells include some population of CBCs ($Lgr5^{high}$) ISCs, position 4+ ISCs (TERT+ and Bmi1+), and TA progenitor ($Lgr5^{low}$) cells.

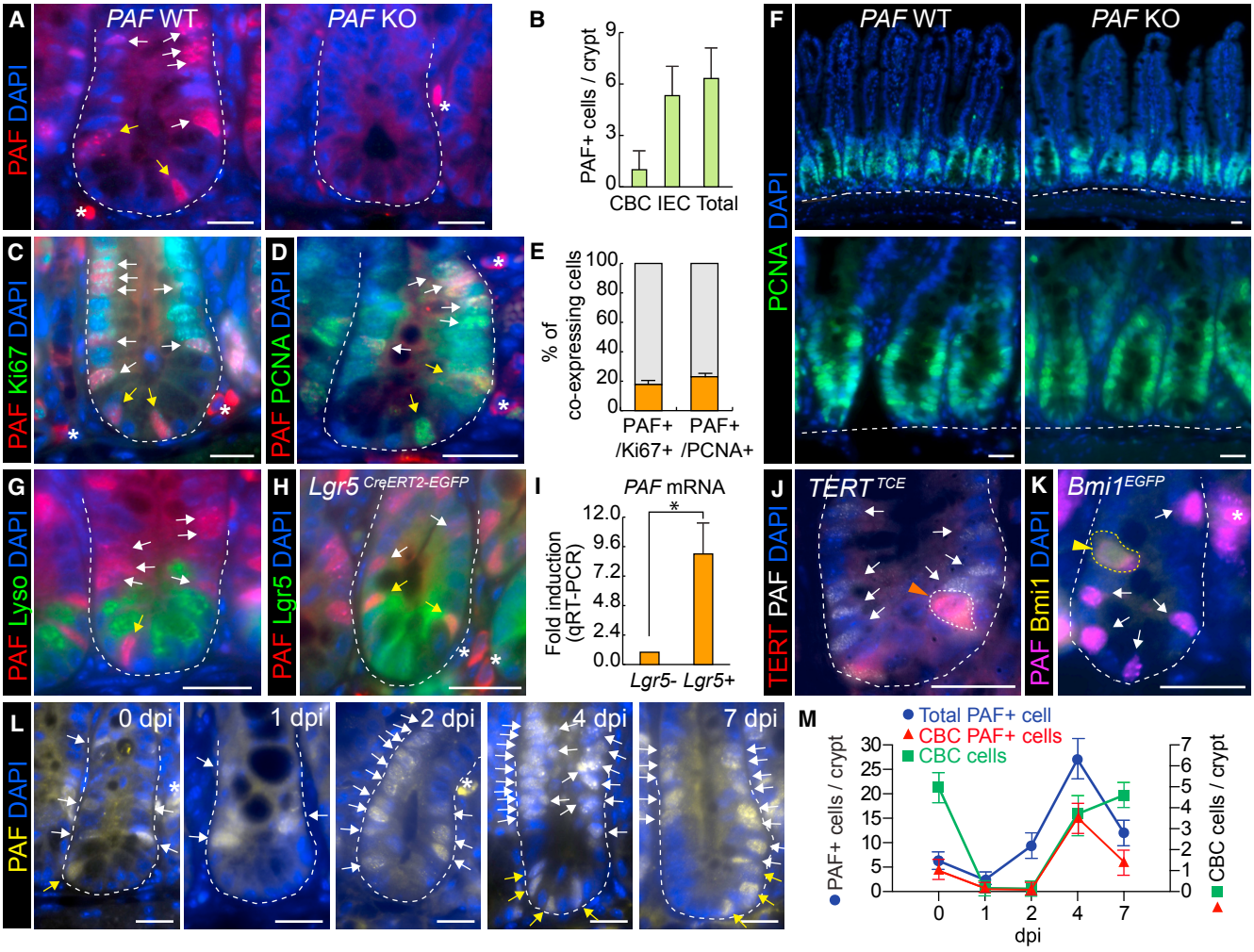

Figure 2. PAF Expression in Normal and Regenerating Intestinal Crypts

(A) PAF expression in the small intestine. *PAF* WT and KO mice were analyzed for immunofluorescent (IF) staining of PAF (arrows).

(B) Quantification of PAF+ cells in the small intestinal crypts.

(C) Co-immunostaining of mouse small intestine (*PAF* WT and KO) for PAF and Ki67. White arrows, PAF+:Ki67+ cells; yellow arrows, PAF+:Ki67+ CBCs.

(D) Co-immunostaining of mouse small intestine (*PAF* WT and KO) for PAF and PCNA. White arrows, PAF+:PCNA+ cells; yellow arrows, PAF+:PCNA+ CBCs.

(E) Quantification of PAF+ cells in K67+ or PCNA+ cell population. Of note, PAF+:Ki67– cells were rarely found (approximately 1/50 crypts).

(F) No effects of *PAF* KO on PCNA expression pattern. IF staining of the mouse small intestine for PCNA.

(G) No expression of PAF in the Paneth cells. Co-immunostaining of the small intestine for PAF and lysozyme. White arrows, PAF+ cells; yellow arrows, PAF+ CBCs.

(H) Co-expression of PAF and Lgr5 in the small intestine. Co-immunostaining of the small intestine of *Lgr5-EGFP-CreERT2* mouse strain. White arrows, PAF+:Lgr5+ cells; yellow arrows, PAF+:Lgr5+ CBCs.

(I) *PAF* expression in Lgr5+ cells. FACS-isolated Lgr5+ cells were analyzed for qRT-PCR. *$p < 0.05$.

(J and K) PAF expression in TERT+ and Bmi1+ cells. Co-immunostaining of *TERT-Tdtomato-CreERT2* or *Bmi1-EGFP* knockin mouse intestine samples for PAF. Arrowheads, PAF+:TERT+ (J) and PAF+:Bmi1+ (K) cells; arrows, PAF+ cells.

(L and M) The increase of PAF+ cells upon radiation injury. Immunostaining of mouse intestine (0, 1, 2, 4, and 7 dpi; 10 Gy) for PAF (L). White arrows, PAF+ cells; yellow arrows, PAF+ CBCs. Quantification of PAF+ cells in the regenerating crypts (M).

The dashed lines indicate the outline of crypts. Asterisks mark non-specific staining signals. Representative images are shown from at least three independent experiments. Scale bars, 20 μm. See also Figures S1 and S2.

Given the upregulation of *PAF* expression by IR (Figure 1), we monitored PAF+ cells in the regenerating intestinal crypts. Interestingly, upon IR exposure (10 Gy), the number of PAF+ cell was increased until 4 dpi and then decreased at 7 dpi (Figures 2L and 2M), which is consistent with *PAF* mRNA upregulation (Figures 1C and 1D). At 1–2 dpi, the remaining ISCs started to divide. At 4 dpi, the regenerating crypts were enlarged, and newly generating CBCs and TA cells reappeared. At 7 dpi, the regeneration process was mostly completed (Jun et al., 2016; Suh et al., 2017). Intriguingly, PAF+ cells remained at position 4–6 and 8–9 at 1–2 dpi, whereas PAF+ CBCs were lost by cell death at 1 dpi (Figures 2L and 2M). The newly generated CBCs and TA cells highly expressed PAF at 4 dpi, and PAF+ cells were partially restored as CBCs and TA cells (7 dpi) (Figures 2L and 2M). Given

the high enrichment of PAF expression in the remaining and active ISCs/IPCs in the regenerating crypts, these results imply that PAF might be involved in controlling ISCs/IPCs during regeneration.

Impaired Intestinal Regeneration by *PAF* KO

To directly test whether PAF is engaged in intestinal regeneration, we utilized a *PAF* KO mouse model. Prior to the experiments, we examined the intestinal morphology and several differentiated intestinal epithelial cell (IEC) markers in *PAF* KO mice. *PAF* KO mice displayed no differences in intestinal morphology and IEC differentiation (Figures S3A and S3B). To further address whether *PAF* KO affects intestinal homeostasis, we performed bromodeoxyuridine (BrdU) incorporation assays (Figures S3C and S3D). The number of BrdU-incorporated cells in the crypts of *PAF* KO mice was the same as that in WT after 2 hr BrdU induction (Figure S3C). Furthermore, *PAF* KO mice showed a similar migration rate during 3 days of tracing of BrdU+ cells (Figure S3D). These data indicate that genetic ablation of *PAF* does not affect the proliferation and migration of IECs. In addition, we analyzed the expression of various genes related to intestinal homeostasis by qRT-PCR (Figure S3E). Despite the slight decrease of c-*Myc* expression in *PAF* KO intestine (~36%), the expression of most genes was not altered in the crypts of WT and *PAF* KO mice. It is noteworthy that conditional deletion of c-*Myc* in the intestine has no impact on intestinal homeostasis (Bettess et al., 2005). These results suggest that PAF is dispensable for intestinal homeostasis.

Next, we asked whether PAF is required for tissue regeneration. We found that, upon IR injury, *PAF* KO mice showed severe defects in the intestinal regeneration (Figures 3A–3D). At 4 dpi, the number of viable crypts was markedly reduced by 10 Gy (50.5% decrease) and 12 Gy (100% decrease) IR treatment (Figures 3B and 3E). The crypt structure, represented by lysozyme staining, was also severely disintegrated in *PAF* KO mice (Figures 3D and 3F) compared with that in WT mice. These results suggest that PAF is indispensable for intestinal regeneration.

PAF Is Required for ISC/IPC Expansion in Regenerating Crypts

To understand the underlying mechanism of intestinal regeneration defects by *PAF* KO, we first examined the DNA repair process in *PAF* KO mice. Interestingly, no significant increase of cell death (apoptotic body and active caspase-3 staining) was detected in *PAF* KO mice during 48 hr after IR (Figures S4A–S4D). Initial recognition of DNA damages, checked by ATM pS1981 (1 hr) and phospho-γ-H2AX (6 hr) (Figures S4E–S4G), and downstream targets of DNA damage responses were not changed in *PAF* KO mice (Figures S4H–S4K). DNA double-strand breaks repair (6–48 hr after IR) represented by γ-H2AX was also similar between *PAF* WT and KO mouse intestine samples (Figures S4E and S4F). These data suggest that regeneration defects in *PAF* KO mice are not due to impaired DNA repair processes.

Next, given the specific expression of PAF in ISCs/IPCs (Figures 2H–2K), we asked whether *PAF* KO-induced defects in intestinal regeneration is due to the dysfunction of ISCs/IPCs. To test this, we performed crypt organoid culture assays. Interestingly, the crypt organoids derived from *PAF* KO mice showed a low efficiency of organoid formation (Figures 4A and 4B), as well as decreased growth and budding efficiency (Figures 4A, 4C, and 4D). These results imply that PAF might be required for intestinal regeneration possibly by controlling ISCs/IPCs in a cell-autonomous manner.

To further assess the underlying mechanisms of dysregulated ISCs/IPCs in *PAF* KO mice during intestinal regeneration, we generated *PAF* KO;*Lgr5-EGFP-CreERT* mice and analyzed the Lgr5+ ISC/IPC population after radiation injury. After IR treatment, $Lgr5^{high}$ ISCs are depleted by DNA damage-induced apoptosis. However, a small population of $Lgr5^{low}$ cells (including quiescent ISCs and TA progenitor cells) survives and contributes to intestinal regeneration (Buczacki et al., 2013; Metcalfe et al., 2014; Muñoz et al., 2012). In the normal intestine of *PAF* KO mice, the number of Lgr5+ ISCs/IPCs was not changed (Figures S5A and S5B), which is consistent with the BrdU incorporation assay results (Figures S3C and S3D). Similarly, *PAF* KO did not affect the number of $Lgr5^{low}$ cell population upon IR (Figures S5C and S5D), suggesting that *PAF* KO has no effects on Lgr5+ ISCs/IPCs with regard to the overall cell viability in the early stage of regeneration (1 dpi, 10 Gy). However, *PAF* KO mice exhibited significantly delayed restoration of Lgr5+ cells in regenerating crypts at the late time point (7 dpi) (Figures 4E–4H). Of note, in the treatment with 10 Gy IR, *PAF* KO mice displayed about 50% of viable crypts (4 dpi) (see Figures 3A–3E). Although the regenerating crypts restored their morphology similar to WT in *PAF* KO mice (7 dpi), the number of Lgr5+ cells was not restored. To complement the *in vivo* result of *PAF* KO-decreased Lgr5+ ISCs/IPCs, we also employed single-cell organoid cultures of FACS-isolated Lgr5+ cells from the mouse intestine. Strikingly, single-cell organoids from *PAF* KO Lgr5+ cells showed three times lower efficiency in the organoid formation, and displayed severe growth defects compared with *PAF* WT Lgr5+ organoids (Figures 4I–4K). *PAF* KO Lgr5+ cells grew markedly slowly during the 2 weeks in single-cell organoid culture. These *in vivo* and *in vitro* results suggest that PAF is required for the expansion of ISCs/IPCs during intestinal regeneration.

PAF Transactivated *c-Myc* Is Required for ISC/IPC Expansion upon Radiation Injury

Next, we sought to determine the molecular mechanism of PAF-induced ISC/IPC expansion. We collected the remaining Lgr5+ cells from IR-treated intestine samples of *Lgr5-EGFP-CreERT* and *PAF* KO mice, and examined the expression of target genes of the Wnt, Notch, Hippo-YAP, Hedgehog, and transforming growth factor β (TGF-β)/bone morphogenic protein pathways (Figures 4L and S5E). In the regenerating crypts (1 and 2 dpi), remaining $Lgr5^{low}$ cells from *PAF* KO mice exhibited a marked decreased expression of Wnt target genes (c-*Myc, Cyclin D1,* and *Lgr5*) (Figures 4L and S5E). The well-established Wnt target gene, *Axin2*, was also decreased in the remaining $Lgr5^{low}$ cells at 2 dpi. Downregulation of Wnt target genes was also observed in the fraction of whole crypts at the late time point (4 dpi) (Figure S5F). IHC confirmed that *c-Myc* and *Cyclin D1* expression was significantly downregulated in 4 dpi *PAF* KO mouse intestine (Figures 5A, 5B, and S5G–S5I). In addition, we found notable PAF+:Myc+ cells in positions 4–6 at 1 dpi, when ISCs are activated for repopulation (Figure 5C). Whereas c-Myc expression

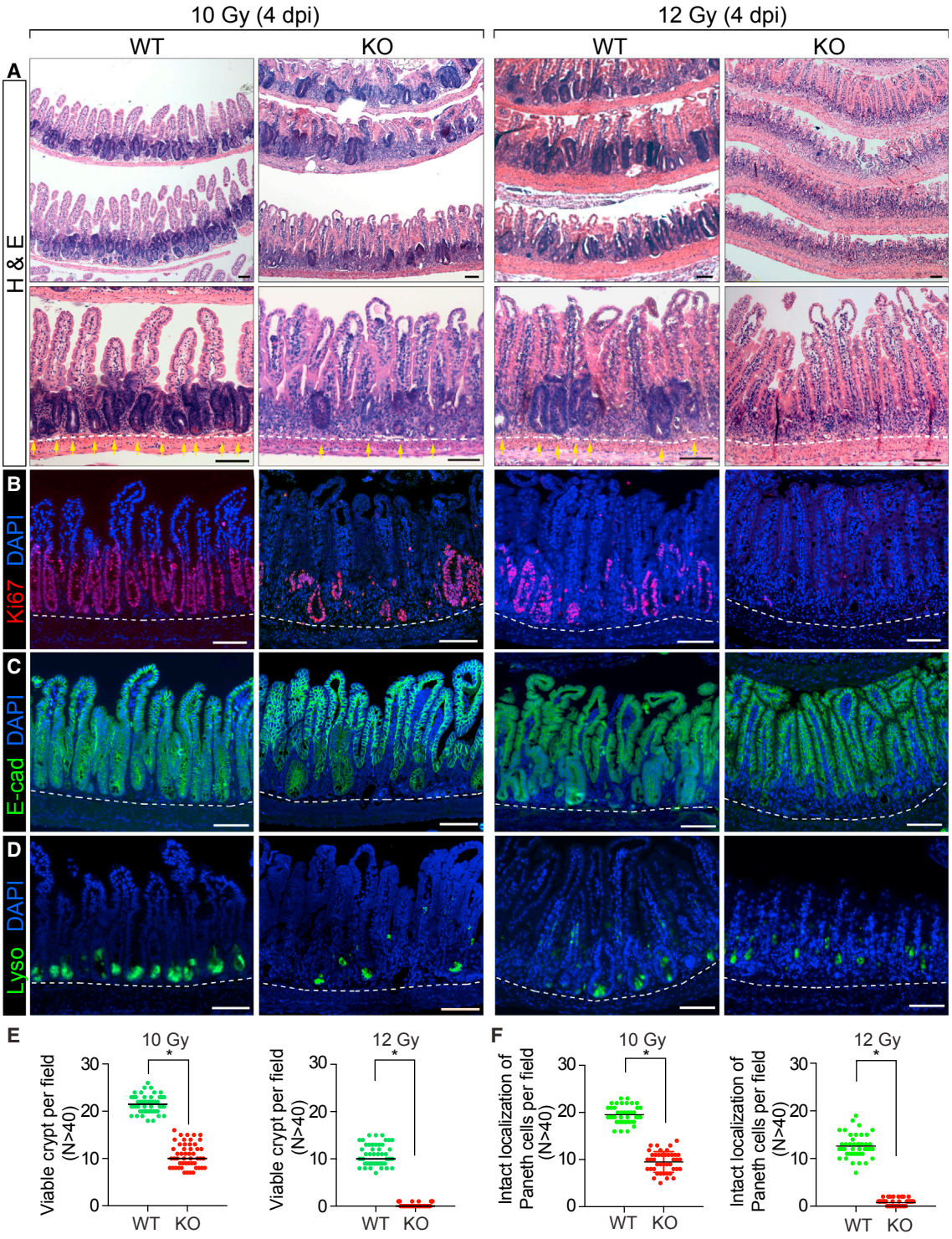

Figure 3. Impaired Intestinal Regeneration by *PAF* KO

(A–D) Impaired intestinal regeneration after irradiation (4 dpi; 10 and 12 Gy). H&E staining of the mouse small intestine samples of $PAF^{+/+}$ (WT) or $PAF^{-/-}$ (KO) mice (A); IHC of the small intestine samples for Ki67 (B); IHC of the small intestine samples for E-cadherin, a marker for epithelial cell (C); IHC of the small intestine samples for lysozyme, a marker for Paneth cell (D); Yellow arrows, crypts.

(E) Quantification of the viable crypts. Crypts that showed five successive Ki67+ cells were counted as a viable crypt. *$p < 0.001$.

(F) Quantification of the intact localization of lysozyme. Crypts possessing at least three Lyso+ cells localized at the crypt bottom were counted as intact localization. *$p < 0.001$.

Representative images are shown from at least three animals for each condition. Scale bars, 100 μm. See also Figures S3 and S4.

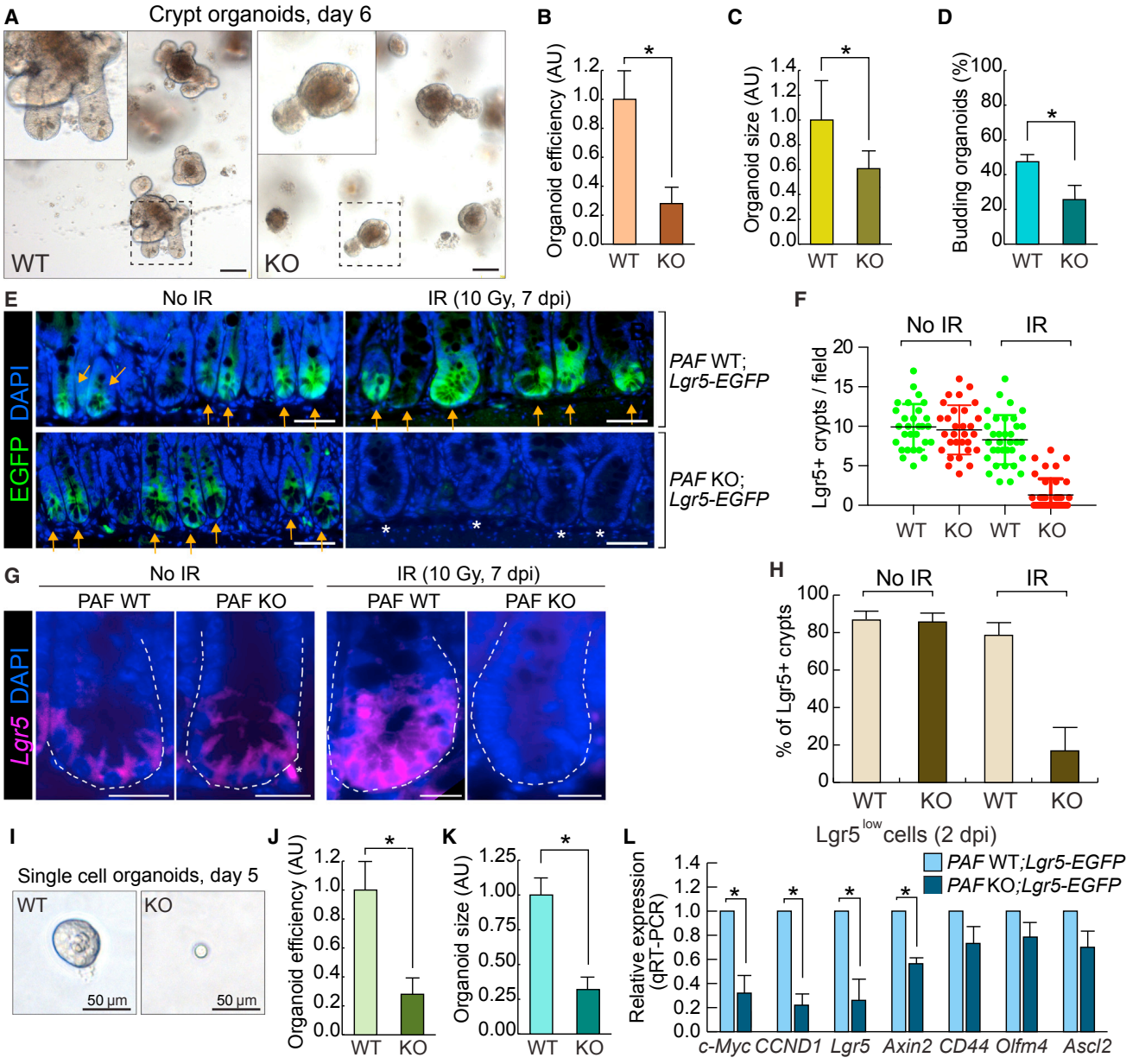

Figure 4. PAF Is Required for ISC/IPC Expansion in Regenerating Crypts

(A–D) Reduced organoid development by *PAF* KO. The crypt organoid growth assays from the small intestine samples of *PAF* WT and KO mice (A); quantification of organoid efficiency ($n \geq 2000$ from the three independent experiments) (B); size (5 days after seeding; $n \geq 50$) (C); budding efficiency ($n \geq 50$) (D). *$p < 0.01$. Scale bars, 100 μm.

(E and F) Impaired ISC/IPC expansion by *PAF* KO. Visualization of Lgr5+ EGFP cells by GFP immunostaining of the small intestines from *PAF* WT;*Lgr5-EGFP* and *PAF* KO;*Lgr5-EGFP* mice at 0 and 7 dpi (E). Scale bars, 50 μm. Quantification Lgr5+ (EGFP+) existing crypts per field (F). At least 30 fields of view were counted; Arrows, EGFP+ crypts; asterisks, EGFP-regenerating crypts.

(G and H) Analysis of *Lgr5* expression by FISH in *PAF* WT and *PAF* KO regeneration crypts. Representative images are shown (G). Scale bars, 20 μm. Percent of Lgr5+ (EGFP+) crypts in the field (H). At least 10 fields of view were counted.

(I–K) Reduced single-cell organoid development by *PAF* KO. Representative images of single-cell (Lgr5+) organoids (day 5) derived from *PAF* WT;*Lgr5-EGFP* and *PAF* KO;*Lgr5-EGFP* mice (I). Scale bars, 50 μm. Quantification of organoid development efficiency (J) ($n \geq 5,000$ cells were analyzed for from three independent experiments); size (K) ($n \geq 30$ single-cell organoids were analyzed). *$p < 0.05$.

(L) Gene expression analysis of FACS-isolated $Lgr5^{low}$ (GFP+) cells in the IR-treated intestine from *PAF* WT;*Lgr5-EGFP* and *PAF* KO;*Lgr5-EGFP* mice (2 dpi, 10 Gy). qRT-PCR analysis. *$p < 0.05$. See also Figure S5.

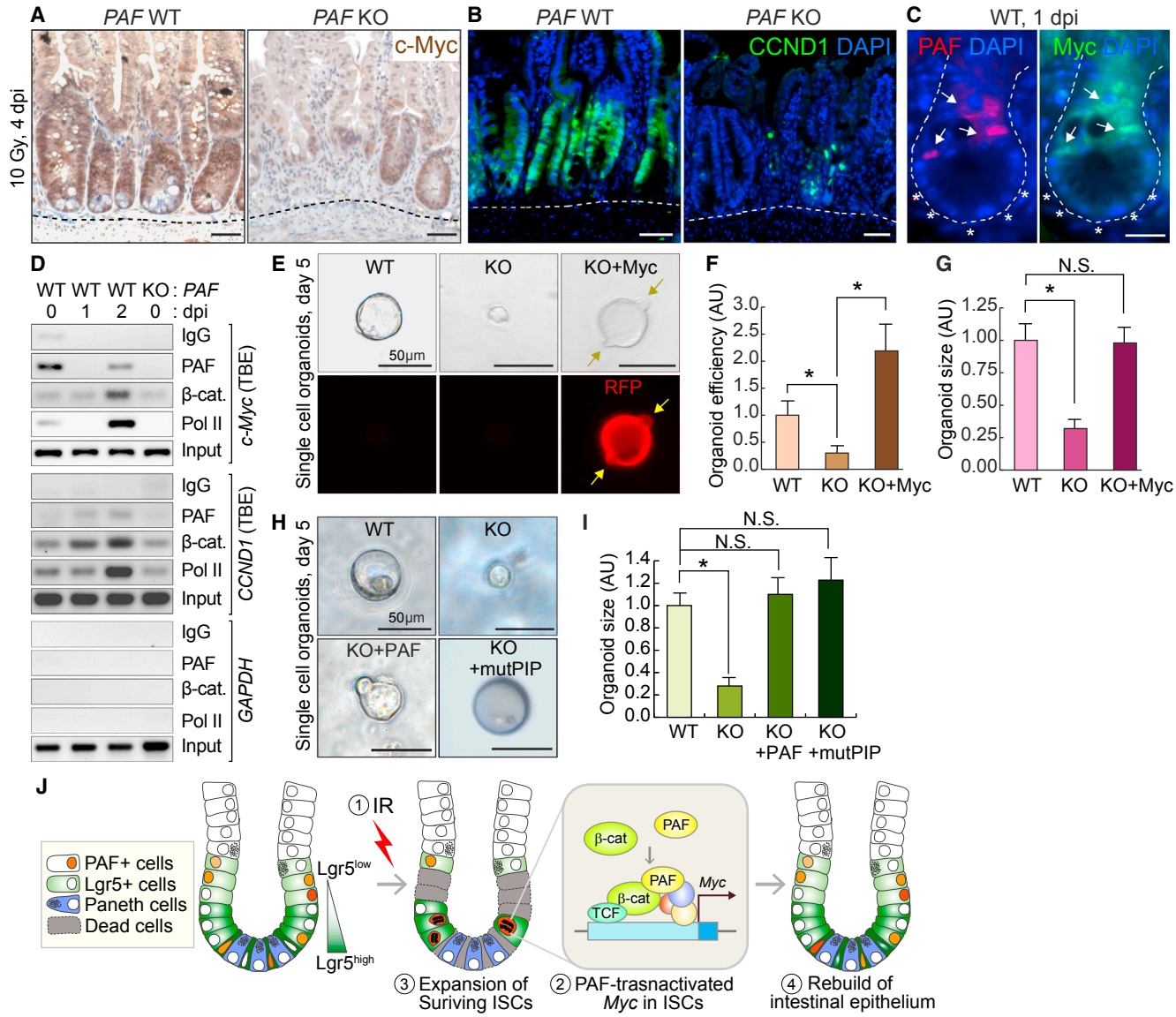

Figure 5. Requirement of PAF-Myc Axis for ISC/IPC Expansion

(A and B) Downregulation of c-Myc and Cyclin D1 in *PAF* KO crypts (4 dpi, 10 Gy). IHC for c-Myc or Cyclin D1. Hematoxylin or DAPI for nuclear counter-staining (blue).

(C) Co-expression of PAF and c-Myc in surviving cells in the regenerating crypts. Arrows, PAF+:Myc+ cells; asterisks, disappeared CBCs.

(D) Conditional recruitment of PAF and β-catenin to TCF-binding elements (TBEs) in *c-Myc* and *CCND1* (*Cyclin D1*) proximal promoter. Chromatin immunoprecipitation (ChIP) assays of the mouse small intestine (*PAF* WT and KO; 1 and 2 dpi; 10 Gy). Immunoglobulin G (IgG) ChIP and *PAF* KO small intestine samples served as negative control. RNA Pol II ChIP (positive control for gene transactivation). *GAPDH* promoter served as negative control.

(E–G) Rescue of *PAF* KO-induced organoid growth failure by c-Myc expression. The Lgr5+ cells isolated from (*PAF* WT and KO) were transduced with retroviruses encoding c-Myc and red fluorescent protein (RFP) and cultured for organoid development. Arrows indicate the budding. Representative images (E); quantification of organoid efficiency (F) and size (G). *$p < 0.05$ ($n \geq 30$). N.S., not significant.

(H and I) Rescue of *PAF* KO-induced organoid growth failure by ectopic expression of wild-type PAF and PIP mutant PAF (mutPIP-PAF). The Lgr5+ cells isolated from *PAF* KO;*Lgr5-EGFP* were transduced with retroviruses encoding wild-type PAF and mutPIP-PAF and cultured for organoid development. Representative images (H); quantification of organoid size (I). *$p < 0.05$ ($n \geq 20$).

(J) Illustration of the working model. Upon irradiation injury, the highly proliferative cells ($Lgr5^{high}$ ISCs and some of $Lgr5^{low}$ TA cells) undergo apoptosis. PAF and β-catenin transactivate *c-Myc* in the surviving ISCs/IPCs ($Lgr5^{low}$), which leads to the expansion of ISCs/IPCs and the subsequent rebuilding of the intestinal epithelium.

Scale bars, 50 μm (A, B, E, and H) and 20 μm (C). Representative images are shown from at least three independent experiments. See also Figure S5.

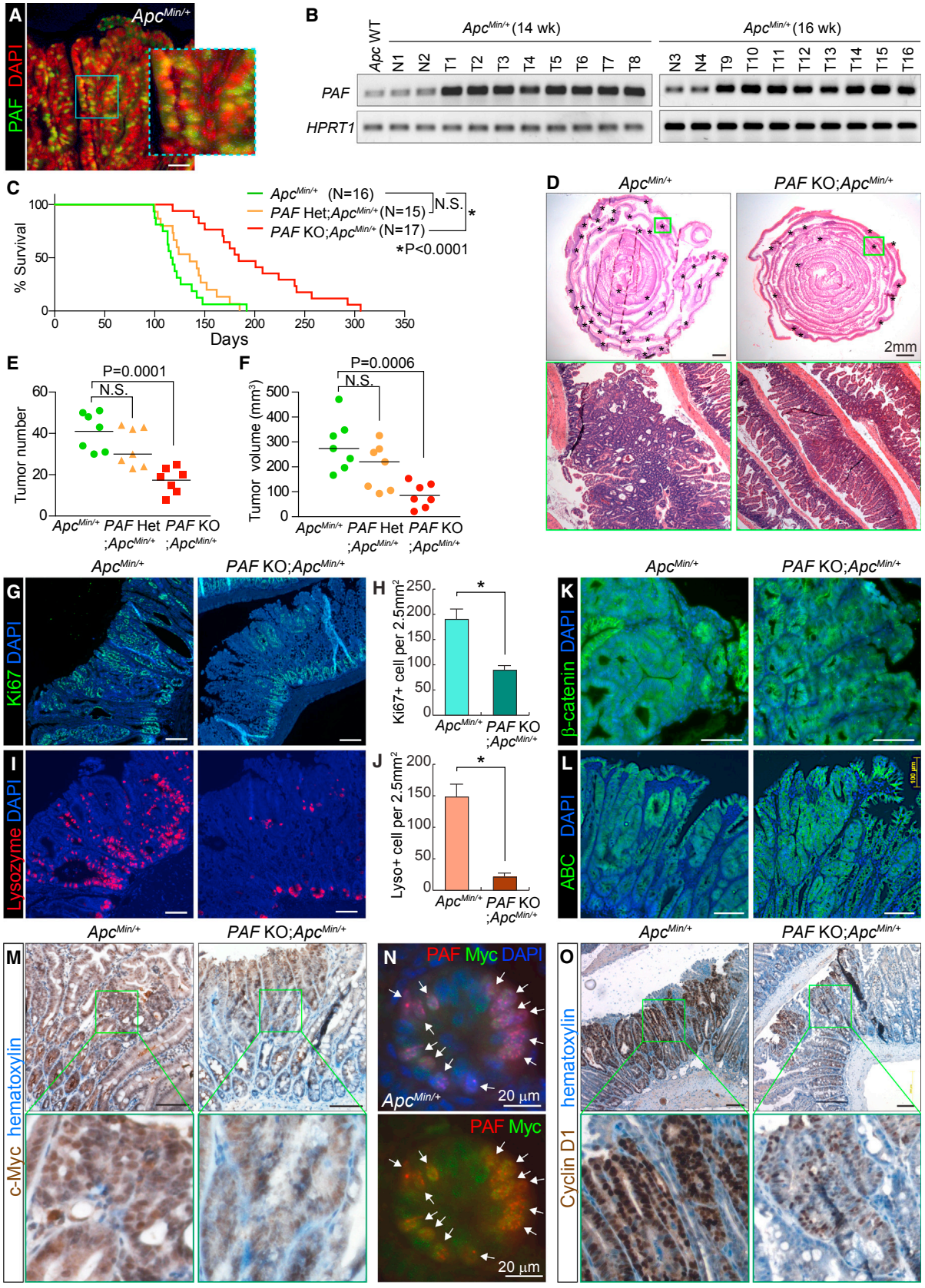

(legend on next page)

was upregulated during regeneration, *PAF* KO showed a decrease in c-Myc expression (Figures S5G–S5I). These results suggest that PAF might be required for c-Myc upregulation during intestinal regeneration.

As a co-factor of β-catenin transcription complex, PAF upregulates c-Myc expression in CRCs (Jung et al., 2013), which led us to determine whether PAF transactivates *c-Myc* in the regenerating intestine. To test this, we performed a chromatin immunoprecipitation assay of the mouse small intestine using PAF antibody. The small intestine samples from *PAF* KO mice served as a negative control (Figure 5D; lane 4). We found that endogenous PAF occupied the TCF-binding element (TBE)-containing proximal promoter of *c-Myc* and *CCND1* (*Cyclin D1*) in the normal intestine (Figure 5D; lane 1, 0 dpi). It is noteworthy that, despite the massive death of PAF+ cells upon IR, some PAF+ cells survived at 1 dpi (Figures 2L and 2M). Nonetheless, we found that IR conditionally induced the recruitment of PAF and β-catenin to the *c-Myc* promoter (Figure 5D; lane 3, 2 dpi). These results suggest that PAF is conditionally associated with and transactivates the *c-Myc* promoter during intestinal regeneration, similar to PAF-induced *c-Myc* transactivation in CRCs (Jung et al., 2013).

Next, we asked whether c-Myc mediates PAF-controlled ISC/IPC expansion by rescue assay of the Lgr5+ single-cell organoid culture. We found that ectopic expression of c-Myc using retrovirus rescued the reduction of organoid-forming efficiency and proliferation in *PAF* KO Lgr5+ organoids (Figures 5E–5G). These results suggest that PAF-transactivated *c-Myc* is required for ISC/IPC expansion during intestinal regeneration.

In addition, we performed rescue experiments using WT PAF and PIP mutant PAF (mutPIP-PAF) (Jung et al., 2013). It has been suggested that the function of PAF in DNA repair is mediated by the interaction of PAF with PCNA via PIP, a PCNA-interacting protein motif (Emanuele et al., 2011; Povlsen et al., 2012). However, mutPIP-PAF expression was sufficient to recover *PAF* KO single-cell organoids (Figures 5H and 5I), suggesting that PAF-mediated DNA repair through PCNA binding is not involved in growth defect of *PAF* KO organoids.

Attenuation of Intestinal Tumorigenesis by *PAF* KO

PAF is significantly upregulated in many human cancers (Cheng et al., 2013; Hosokawa et al., 2007; Jain et al., 2011; Jun et al., 2013; Jung et al., 2013; Kais et al., 2011; Kato et al., 2012; Mizutani et al., 2005; Wang et al., 2016; Yu et al., 2001; Yuan et al., 2007), indicating the potential roles of PAF in promoting tumorigenesis. In addition, given the pivotal roles of PAF and c-Myc in controlling ISC/IPC activation (Figures 5 and S5G–S5I) and initiating intestinal tumorigenesis (Jung et al., 2013; Sansom et al., 2007), we next asked whether PAF contributes to intestinal tumorigenesis by positively modulating the cancer cell stemness. We assessed the expression of *PAF* in intestinal adenomas driven by *Apc* mutation using $Apc^{Min/+}$ mouse model (Moser et al., 1990). IHC results showed that PAF was markedly upregulated in intestinal adenomas of $Apc^{Min/+}$ mice (Figure 6A). Semi-quantitative RT-PCR of individually isolated intestinal adenomas and adjacent normal intestine samples of $Apc^{Min/+}$ mice (age of 14 and 16 weeks) also showed the marked upregulation of *PAF* in *Apc* mutation-driven adenomas (Figure 6B), which confirms the upregulation of PAF in CRC (Jung et al., 2013). Of note, PAF+ cells were a subpopulation of Ki67+ or PCNA+ cells in adenomas (27.68% and 26.49%, respectively) (Figures S6A–S6D).

To test whether genetic ablation of *PAF* suppresses tumorigenesis in a mouse model, we established $Apc^{Min/+}$ (control group) and *PAF* KO;$Apc^{Min/+}$ compound strains (experimental group). The median survival of $Apc^{Min/+}$ mice was 117 days (n = 16). Surprisingly, *PAF* KO;$Apc^{Min/+}$ mice displayed marked extended survival (median 184 days, n = 17; p = 0.0001) (Figure 6C). Moreover, *PAF* KO;$Apc^{Min/+}$ mice showed a decreased number and size of adenomas, compared with those in $Apc^{Min/+}$ mice (Figures 6D, 6F, and S6E). Of note, *PAF* heterozygous KO (*PAF* Het;$Apc^{Min/+}$) did not affect mouse survival or the number and size of adenomas compared with *PAF* KO;$Apc^{Min/+}$ (Figures 6C–6F). Ki67 IHC showed reduced cell proliferation in adenomas developed in *PAF* KO;$Apc^{Min/+}$ mice compared with that in $Apc^{Min/+}$ control mice (Figures 6G and 6H). The number of Paneth cells was also diminished in intestinal adenomas of *PAF* KO;$Apc^{Min/+}$ mice (Figures 6I and 6J). Given that the Paneth cell differentiation is driven by Wnt/β-catenin signaling (van Es et al., 2005), it is possible that *PAF* KO might induce the overall downregulation of Wnt/β-catenin target genes in tumor cells. Based on our previous finding that PAF hyperactivates the Wnt signaling as a co-factor of the β-catenin transcriptional complex (Jung et al., 2013), we tested whether *PAF* KO suppresses

Figure 6. Attenuation of Intestinal Tumorigenesis by *PAF* KO

(A and B) Expression of PAF in Apc^{Min} adenomas. Immunostaining of $Apc^{Min/+}$ intestinal adenoma (16 weeks old) (A). Scale bar, 50 μm. Semiquantitative RT-PCR (B). *Apc* WT, wild-type ($Apc^{+/+}$) intestine sample; N1-4, normal adjacent intestine samples; T1-16, intestinal adenomas.

(C) The extended life span of $Apc^{Min/+}$ mice by *PAF* KO. Kaplan-Meier survival curve of $Apc^{Min/+}$ (n = 16), *PAF* Het;$Apc^{Min/+}$ (n = 15), and *PAF* KO;$Apc^{Min/+}$ (n = 17).

(D) H&E staining of the small intestines from $Apc^{Min/+}$ and *PAF* KO;$Apc^{Min/+}$ (age of 16 weeks). Asterisks indicate intestinal adenomas. Scale bars, 2 mm.

(E and F) Decreased tumor burden of $Apc^{Min/+}$ mice by *PAF* KO. The number of tumors (≥1.5 mm) (E) and tumor volumes (mm^3) (F) were quantified; 16 weeks old; n = 7 for each group.

(G and H) Reduced cell proliferation of Apc^{Min} tumors by *PAF* KO. Ki67 staining of small intestine adenomas from $Apc^{Min/+}$ or *PAF* KO;$Apc^{Min/+}$ (16 weeks old) (G); quantification (H). Scale bars, 100 μm. *p < 0.001.

(I and J) Decreased differentiation of the Paneth cells of Apc^{Min} tumors by *PAF* KO. Lysozyme staining of small intestine adenomas from $Apc^{Min/+}$ or *PAF* KO;$Apc^{Min/+}$ (16 weeks old) (I); quantification (J). Scale bars, 100 μm. *p < 0.001.

(K and L) No change in β-catenin level and activity of Apc^{Min} tumors by *PAF* KO. Immunostaining of small intestine adenomas from $Apc^{Min/+}$ or *PAF* KO;$Apc^{Min/+}$ (16 weeks old) for total β-catenin (K) and active (unphosphorylated) β-catenin (ABC) (L). Scale bars, 100 μm.

(M) Downregulation of c-Myc of Apc^{Min} tumors by *PAF* KO. c-Myc IHC; 16 weeks old. Scale bars, 100 μm.

(N) Co-expression of c-Myc and PAF in Apc^{Min} tumors. Arrows, PAF+:Myc+ cells. Scale bars, 20 μm.

(O) Downregulation of cyclin D1 of Apc^{Min} tumors by *PAF* KO. Cyclin D1 IHC; 16 weeks old. Scale bars, 100 μm.

Representative images (n ≥ 3) are shown. See also Figure S6.

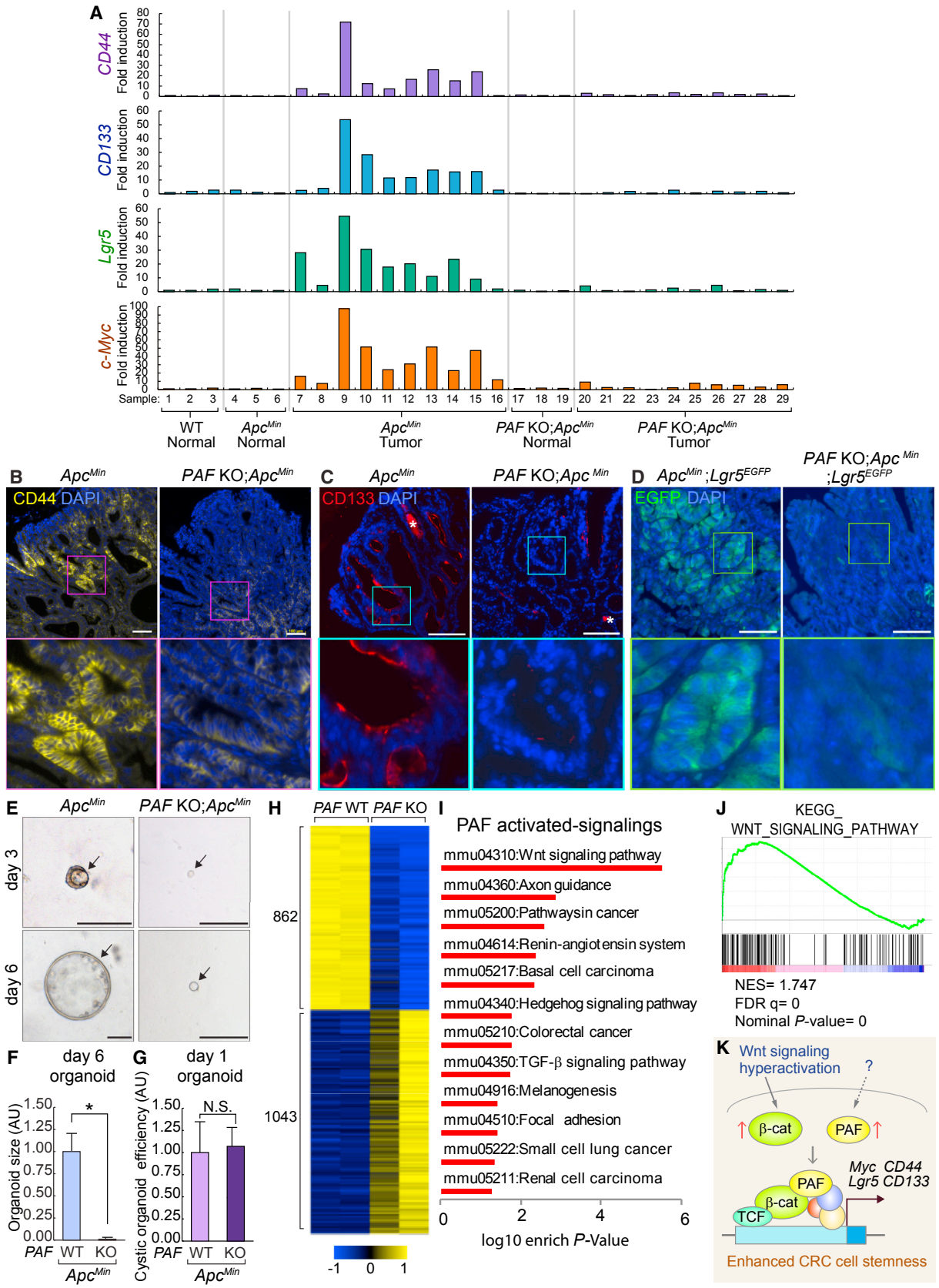

(legend on next page)

Wnt/β-catenin signaling in intestinal adenomas. While *PAF* KO did not affect the level and activity of the β-catenin protein in adenomas (Figures 6K and 6L), *PAF* KO notably downregulated the expression of Wnt/β-catenin target genes, c-Myc and Cyclin D1, in intestinal adenomas (Figures 6M–6O and S6G). Furthermore, we found that PAF was co-expressed with c-Myc in intestinal adenomas of $Apc^{Min/+}$ mice, similar to their co-expression in the regenerating crypts (Figures 6N and S6F). These results suggest that *PAF* KO attenuates intestinal tumorigenesis by downregulation of β-catenin target genes, including c-Myc.

Reduced CRC Cell Stemness by *PAF* KO

Previously, we found that the PAF-Wnt signaling axis is required for the maintenance of breast cancer cell stemness (Wang et al., 2016). Moreover, having determined that PAF is indispensable for ISC/IPC expansion in regeneration (Figures 4), we next examined the role of PAF in controlling the stemness of CRCs. We analyzed the expression of several known CRC stemness makers (CD44, CD133, and Lgr5) (O'Brien et al., 2007; Ricci-Vitiani et al., 2007; Schepers et al., 2012; Zeilstra et al., 2008; Zhu et al., 2009). Adenomas from *PAF* KO;$Apc^{Min/+}$ mice showed marked decreased expression of CRC stemness markers (CD44, CD133, and Lgr5) (Figures 7A–7D, S7A, and S7B). To better understand the role of PAF in CRC stemness, we cultured tumor organoids from $Apc^{Min/+}$ and *PAF* KO;$Apc^{Min/+}$ crypts. Owing to hyperactivation of Wnt signaling, $Apc^{Min/+}$ organoids develop into a spherical shape (cystic) without budding (Sato et al., 2011a). Surprisingly, the organoids derived from *PAF* KO;$Apc^{Min/+}$ mouse intestine showed severe defects in growth (Figures 7E and 7F). Although the initial organoid forming efficiency was similar (Figure 7G), *PAF* KO; $Apc^{Min/+}$ organoids did not grow until 21 days, compared with the organoids from *PAF* WT;$Apc^{Min/+}$ (Figures 7E and 7F). One copy deletion of PAF (*PAF* Het;$Apc^{Min/+}$) did not suppress the cystic organoid growth (Figure S7C), consistent with *in vivo* results from *PAF* Het; $Apc^{Min/+}$ mice (see Figures 6C–6F). We further assessed the effects of PAF knockdown on cancer cell stemness using human CRCs. Colorectal CSCs exhibit enrichment of CD44 and CD133 expression (Kemper et al., 2010; O'Brien et al., 2007; Ricci-Vitiani et al., 2007). We found a significantly decreased population of CD44+:CD133+ cells in PAF-depleted HT29 cells (Figure S7D). Furthermore, PAF knockdown inhibited colonosphere formation of HT29 (Figures S7E and S7F). These results suggest that PAF is required for the maintenance of CRC stemness.

Next, for an unbiased assessment of PAF-controlled transcriptome in intestinal tumors, we also performed RNA sequencing (RNA-seq) of *PAF* WT and KO Apc^{Min} mouse tumors (Figure 7H). Kyoto Encyclopedia of Genes and Genomes analysis showed that Wnt signaling is markedly downregulated in *PAF* KO tumor cells (Figures 7I and S7G; Table S1), which was also confirmed by gene set enrichment analysis (GSEA) (Figure 7J and Table S2). These results strongly suggest that PAF positively modulates Wnt/β-catenin signaling in CRC, similar to that during intestinal regeneration.

DISCUSSION

Herein, our comprehensive approaches revealed that the PAF-Myc axis is required for ISC/IPCexpansion during intestinal regeneration and tumorigenesis.

c-Myc is not required for normal intestine homeostasis, but is indispensable for intestinal regeneration (Ashton et al., 2010; Bettess et al., 2005). However, it was unknown how c-Myc contributes to intestinal regeneration. In our experimental setting, ectopic expression of c-Myc rescued *PAF* KO-induced defects in Lgr5+ single-cell organoid growth (see Figures 5E–5G), which strongly suggests that c-Myc mediates PAF-controlled ISC/IPC expansion during intestinal regeneration. Interestingly, *PAF* KO did not affect intestinal homeostasis, which requires constitutively active Wnt signaling in the crypts. Nonetheless, there were no changes in the expression of Wnt/β-catenin target genes (*Cyclin D1*, *CD44*, and *Lgr5*) in *PAF* KO intestine (without IR injury) (see Figure S3E). However, under specific physiologic or pathologic conditions, such as regeneration or tumorigenesis when enhanced Wnt signaling is required (Cadigan and Waterman, 2012; Clevers and Nusse, 2012; Polakis, 2012), the highly upregulated PAF hyperactivates the Wnt/β-catenin transcriptional complex and transactivates *c-Myc*, which subsequently triggers the activation of self-renewing cells (Figures 5J and 7K). This is also supported by the marked upregulation of PAF expression in the regenerating crypts (see Figures 1A, 1C, and 2L) and CRCs (Jung et al., 2013).

Figure 7. Decreased CRC Cell Stemness by *PAF* KO

(A) Gene expression analysis of *CD44*, *CD133*, *Lgr5*, and *c-Myc* in the normal intestine or adenomas from $Apc^{Min/+}$ and *PAF* KO;$Apc^{Min/+}$ (16 weeks old). At least three individual samples from WT and normal region of $Apc^{Min/+}$ *and PAF* KO;$Apc^{Min/+}$ were used as the control.

(B and C) Downregulation of CD44 and CD133 expression in Apc^{Min} tumors by *PAF* KO. IF staining for CD44 and CD133; 16 weeks old. Asterisks mark nonspecific signal. Scale bars, 100 μm.

(D) Downregulation of Lgr5 in Apc^{Min} tumors by *PAF* KO. IF for GFP (adenomas of $Apc^{Min/+}$;*Lgr5-EGFP* and *PAF* KO;$Apc^{Min/+}$;*Lgr5-EGFP* [16 weeks old]). Scale bars, 100 μm.

(E) Reduced cystic organoid development by *PAF* KO. Representative images of organoids (days 3 and 6, black arrows) derived from Apc^{Min} and *PAF* KO;Apc^{Min} adenomas. Scale bars, 100 μm.

(F and G) Quantification of organoid size at day 6 (F) ($n \geq 30$ cystic organoids were analyzed); efficiency (G) ($n \geq 5000$ cells were analyzed for from three independent experiments). *$p < 0.001$; N.S., not significant.

(H) Heatmap gene expression profile generated by significant differential expression ($p < 0.05$) of Apc^{Min} and *PAF* KO;Apc^{Min} adenomas by RNA sequencing ($n = 2$ per group).

(I) Significantly PAF upregulated signaling pathways identified by gene set enrichment analysis (GSEA) (Kyoto Encyclopedia of Genes and Genomes [KEGG]) using RNA-seq results. $p < 0.05$.

(J) GSEA for Wnt signaling pathway. NES, normalized enrichment score; FDR, false detection rate; p value, nominal p value.

(K) Illustration of the working model. During tumorigenesis, Wnt/β-catenin signaling is hyperactivated and PAF is upregulated. PAF and β-catenin transactivate *c-Myc* and CRC stemness-related genes (CD44, CD133, and Lgr5), which leads to the increase of CRC stemness.

See also Figure S7, Tables S1 and S2.

Accumulating evidence suggests the pivotal roles of c-Myc in regulating stem cells. c-Myc is necessary for efficient cellular reprogramming of induced pluripotent stem cells (iPSCs) (Araki et al., 2011; Takahashi et al., 2007). In ESCs, c-Myc modulates cell stemness and differentiation by amplifying protein biosynthesis (Nie et al., 2012; Varlakhanova et al., 2010). c-Myc also regulates the balance between self-renewing and differentiated/committed hematopoietic stem cells by controlling the interaction with their niche (Laurenti et al., 2008; Wilson et al., 2004). Given the specific and dynamic expression of PAF in ISCs/IPCs (see Figure 2) and PAF-transactivated *c-Myc* (see Figure 5), it is probable that PAF may play pivotal roles in governing various stem cells via c-Myc. Indeed, in the small intestine, *PAF* KO decreased the expression of stem cell marker, Lgr5, in the regenerating crypts accompanied with the downregulation of *c-Myc*. Furthermore, c-Myc rescued *PAF* KO-induced failure of organoid growth (see Figures 5E–5G), indicating that PAF functions as an upstream molecule of c-Myc in controlling the stem cells.

Seventy percent of human CRCs display a significant upregulation of c-Myc (Erisman et al., 1985; Sikora et al., 1987). In mouse models, genetic ablation of *c-Myc* suppresses intestinal tumorigenesis driven by *Apc* mutations (Sansom et al., 2007). Similarly, *PAF* KO inhibits intestinal adenoma development in $Apc^{Min/+}$ mice with reduced c-Myc expression (see Figures 6M and S6G). Moreover, the depletion of *PAF* decreased the expression of CRC stemness markers (CD44, CD133, and Lgr5) in Apc^{Min} adenomas (see Figures 7A–7D) with downregulation of *c-Myc* (see Figures 6M and 7A). Although the effects of *PAF* KO on CRC stemness should be further elaborated with cell ablation, lineage-tracing, and serial transplantation assays, our results are somewhat similar to our previous study that PAF is required for the maintenance of breast cancer cell stemness (Wang et al., 2016). Although Myc depletion rescued phenotypes of tumorigenesis driven by *Apc* mutation in the mouse model (Sansom et al., 2007), the ectopic expression of Myc failed to rescue the organoid growth in *PAF* KO;$Apc^{Min/+}$ condition. These results imply that additional factors/pathways might be involved in PAF-controlled CRC stemness. Transcriptomic analysis of $Apc^{Min/+}$ and *PAF* KO;$Apc^{Min/+}$ adenomas revealed that in addition to Wnt signaling, other oncogenic pathways including Hedgehog and TGF-β signaling were modulated by PAF (Figures 7H–7J and S7H). Given the oncogenic function of Hedgehog and TGF-β signaling in CRC (Munoz et al., 2006; Takaku et al., 1998; Varnat et al., 2009), it is possible that PAF-controlled CRC stemness is mediated by several oncogenic pathways including Wnt-Myc, Hedgehog, and TGF-β signaling. Although we here limited our scope to the PAF-activated Wnt-Myc axis, it is necessary to further examine how PAF is associated with various oncogenic signalings beyond the Wnt/β-catenin pathway.

PAF directly binds to PCNA (De Biasio et al., 2015). Nonetheless, it is highly likely that PAF-controlled stem cells might be independent of PCNA interaction, which is supported by the following results: (1) without IR treatment, *PAF* KO is sufficient to suppress organoid growth (Figures 4A–4D and 4I–4K), which rules out the potential involvement of PAF-mediated DNA repair in tissue regeneration; (2) PAF transactivates β-catenin target genes including c-*Myc* in a PCNA-independent manner (Jung et al., 2013); (3) instead of DNA repair genes, c-Myc is sufficient to rescue the *PAF* KO phenotypes in the single-cell organoid growth (see Figures 5E–5G); (4) ectopic expression of PIP-mutated PAF fully rescues the defect of *PAF* KO organoid growth (see Figures 5H and 5I); (5) only some of PCNA+ cells are PAF+ cells in the normal intestine (26.49%) and adenomas (23.01%) (see Figures 2D, 2E, S6C, and S6D), indicating the potential roles of PAF in a PCNA-independent manner; (6) *PAF* KO mice showed no abnormality in PCNA expression and IEC growth in the crypts (see Figure 2F); (7) *PAF* KO did not affect the DNA double-strand breaks and DNA damage foci formation in the intestine (see Figures S4E and S4F), indicating that PAF is dispensable for genomic stability or DNA repair. Thus, these results strongly support that PAF-mediated intestinal regeneration is independent of the PCNA and DNA repair pathways.

Although PAF+ cells partially mark ISCs and TA cells in the normal intestine, *PAF* KO mice did not display defects in tissue homeostasis (see Figures S3). Tissue injury upregulates PAF expression, which enhances *c-Myc* transcription for the subsequent expansion of ISCs/IPCs. This is also supported by co-expression of PAF and c-Myc in the surviving cells (not the Paneth cells) of regenerating crypts (see Figure 5C). Employing PAF reporter and lineage-tracing mice will provide further insights into how PAF+ cells contribute to tissue regeneration and cancer.

Despite the crucial roles of PAF in regulating self-renewing cells in intestinal regeneration and tumorigenesis, it is still unclear how PAF is upregulated in the regenerating crypts and CRC. Due to the high expression of PAF in $Apc^{Min/+}$ tumors (see Figures 6A and 6B), it is reasonable that Wnt/β-catenin signaling might directly transactivate *PAF*. Although the proximal promoter of *PAF* contains multiple TBEs (Wang et al., 2016), we found that manipulation of Wnt/β-catenin signaling did not affect the transcription of *PAF* in both IECs and CRCs (Figures S7I and S7J). Given our previous finding that Oct4, Nanog, and Sox2 transactivate *PAF* in breast cancer cells and mammary epithelial cells (Wang et al., 2016), the involvement of such iPSC-inducing factors in PAF regulation should be addressed in future studies.

PAF is significantly upregulated in CRC and contributes to tumorigenesis, whereas it is dispensable for tissue homeostasis. Therefore, PAF might be a viable molecular target for cancer treatment with minimal damage to the normal cells. Conversely, tweaking PAF might provide new ways to manipulate tissue regeneration. Collectively, our findings unveil the essential role of the PAF-Myc signaling axis in controlling stem cell activation in regeneration and cancer.

STAR★METHODS

Detailed methods are provided in the online version of this paper and include the following:

- KEY RESOURCES TABLE
- CONTACT FOR REAGENT AND RESOURCE SHARING
- EXPERIMENTAL MODEL AND SUBJECT DETAILS
  - Mouse Strains
- METHOD DETAILS
  - Generation of *PAF* KO Mice
  - Radiation Injury
  - Gene Expression Analysis

- Crypt Organoid Culture
- Organoid Retrovirus Infection
- *Lgr5* mRNA Fluorescence In Situ Hybridization (FISH)
- Mammalian Cell Culture and Sphere Formation Assay
- Chromatin Immunoprecipitation Assay
- RNA-sequencing

- QUANTIFICATION AND STATISTICAL ANALYSIS
- DATA AND SOFTWARE AVAILABILITY

SUPPLEMENTAL INFORMATION

Supplemental Information includes seven figures and three tables and can be found with this article online at https://doi.org/10.1016/j.devcel.2018.02.010.

ACKNOWLEDGMENTS

We are grateful to Christopher Cervantes, Youn-Sang Jung, Seung-Hyo Lee, and Junjie Chen for helpful comments on the manuscript. This work was supported by the Cancer Prevention and Research Institute of Texas (RP140563), the NIH (R01 CA193297-01), the Department of Defense (CA140572), the National Cancer Institute (P50 CA098258), the Duncan Family Institute Research Program, the University Cancer Foundation (IRG-08-061-01), the Center for Stem Cell and Developmental Biology (MD Anderson Cancer Center), an Institutional Research Grant (MD Anderson Cancer Center), a New Faculty Award (MD Anderson Cancer Center Support Grant), a Metastasis Research Center Grant (MD Anderson Cancer Center), and the Uterine SPORE Career Enhancement Program (MD Anderson Cancer Center). The Genetically Engineered Mouse Facility was supported by the MD Anderson Cancer Center Support Grant (CA016672).

AUTHOR CONTRIBUTIONS

M.J.K. and J.-I.P. conceived the experiments. M.J.K., H.N.S., S.H.L., S.J., E.M.L., and J.Z. performed the experiments. B.X. and K.C. analyzed RNA-seq results. M.J.K. and J.-I.P. analyzed the data. M.J.K. and J.-I.P. wrote the manuscript.

DECLARATION OF INTERESTS

The authors declare no competing interests.

Received: March 12, 2017
Revised: December 10, 2017
Accepted: February 7, 2018
Published: March 12, 2018

REFERENCES

Araki, R., Hoki, Y., Uda, M., Nakamura, M., Jincho, Y., Tamura, C., Sunayama, M., Ando, S., Sugiura, M., Yoshida, M.A., et al. (2011). Crucial role of c-Myc in the generation of induced pluripotent stem cells. Stem Cells *29*, 1362–1370.

Asfaha, S., Hayakawa, Y., Muley, A., Stokes, S., Graham, T.A., Ericksen, R.E., Westphalen, C.B., von Burstin, J., Mastracci, T.L., Worthley, D.L., et al. (2015). Krt19(+)/Lgr5(–) cells are radioresistant cancer-initiating stem cells in the colon and intestine. Cell Stem Cell *16*, 627–638.

Ashton, G.H., Morton, J.P., Myant, K., Phesse, T.J., Ridgway, R.A., Marsh, V., Wilkins, J.A., Athineos, D., Muncan, V., Kemp, R., et al. (2010). Focal adhesion kinase is required for intestinal regeneration and tumorigenesis downstream of Wnt/c-Myc signaling. Dev. Cell *19*, 259–269.

Barker, N., Van Es, J.H., Kuipers, J., Kujala, P., Van Den Born, M., Cozijnsen, M., Haegebarth, A., Korving, J., Begthel, H., Peters, P.J., et al. (2007). Identification of stem cells in small intestine and colon by marker gene Lgr5. Nature *449*, 1003–1007.

Bettess, M.D., Dubois, N., Murphy, M.J., Dubey, C., Roger, C., Robine, S., and Trumpp, A. (2005). c-Myc is required for the formation of intestinal crypts but dispensable for homeostasis of the adult intestinal epithelium. Mol. Cell. Biol. *25*, 7868–7878.

Buczacki, S.J.A., Zecchini, H.I., Nicholson, A.M., Russell, R., Vermeulen, L., Kemp, R., and Winton, D.J. (2013). Intestinal label-retaining cells are secretory precursors expressing Lgr5. Nature *495*, 65–69.

Cadigan, K.M., and Waterman, M.L. (2012). TCF/LEFs and Wnt signaling in the nucleus. Cold Spring Harb. Perspect. Biol. *4*, https://doi.org/10.1101/cshperspect.a007906.

Cheng, Y., Li, K., Diao, D., Zhu, K., Shi, L., Zhang, H., Yuan, D., Guo, Q., Wu, X., Liu, D., et al. (2013). Expression of KIAA0101 protein is associated with poor survival of esophageal cancer patients and resistance to cisplatin treatment in vitro. Lab. Invest. *93*, 1276–1287.

Clevers, H., and Nusse, R. (2012). Wnt/beta-catenin signaling and disease. Cell *149*, 1192–1205.

De Biasio, A., de Opakua, A.I., Mortuza, G.B., Molina, R., Cordeiro, T.N., Castillo, F., Villate, M., Merino, N., Delgado, S., Gil-Carton, D., et al. (2015). Structure of p15(PAF)-PCNA complex and implications for clamp sliding during DNA replication and repair. Nat. Commun. *6*, 6439.

Dean, M., Fojo, T., and Bates, S. (2005). Tumour stem cells and drug resistance. Nat. Rev. Cancer *5*, 275–284.

Emanuele, M.J., Ciccia, A., Elia, A.E.H., and Elledge, S.J. (2011). Proliferating cell nuclear antigen (PCNA)-associated KIAA0101/PAF15 protein is a cell cycle-regulated anaphase-promoting complex/cyclosome substrate. Proc. Natl. Acad. Sci. USA *108*, 9845–9850.

Erisman, M.D., Rothberg, P.G., Diehl, R.E., Morse, C.C., Spandorfer, J.M., and Astrin, S.M. (1985). Deregulation of c-myc gene expression in human colon carcinoma is not accompanied by amplification or rearrangement of the gene. Mol. Cell. Biol. *5*, 1969–1976.

Fuchs, E., Tumbar, T., and Guasch, G. (2004). Socializing with the neighbors: stem cells and their niche. Cell *116*, 769–778.

Hosen, N., Yamane, T., Muijtjens, M., Pham, K., Clarke, M.F., and Weissman, I.L. (2007). Bmi-1-green fluorescent protein-knock-in mice reveal the dynamic regulation of bmi-1 expression in normal and leukemic hematopoietic cells. Stem Cells *25*, 1635–1644.

Hosokawa, M., Takehara, A., Matsuda, K., Eguchi, H., Ohigashi, H., Ishikawa, O., Shinomura, Y., Imai, K., Nakamura, Y., and Nakagawa, H. (2007). Oncogenic role of KIAA0101 interacting with proliferating cell nuclear antigen in pancreatic cancer. Cancer Res. *67*, 2568–2576.

Jain, M., Zhang, L., Patterson, E.E., and Kebebew, E. (2011). KIAA0101 is overexpressed, and promotes growth and invasion in adrenal cancer. PLoS One *6*, e26866.

Jun, S., Jung, Y.S., Suh, H.N., Wang, W., Kim, M.J., Oh, Y.S., Lien, E.M., Shen, X., Matsumoto, Y., McCrea, P.D., et al. (2016). LIG4 mediates Wnt signalling-induced radioresistance. Nat. Commun. *7*, 10994.

Jun, S., Lee, S., Kim, H.C., Ng, C., Schneider, A.M., Ji, H., Ying, H., Wang, H., DePinho, R.A., and Park, J.I. (2013). PAF-mediated MAPK signaling hyperactivation via LAMTOR3 induces pancreatic tumorigenesis. Cell Rep. *5*, 314–322.

Jung, H.Y., Jun, S., Lee, M., Kim, H.C., Wang, X., Ji, H., McCrea, P.D., and Park, J.I. (2013). PAF and EZH2 induce wnt/β-catenin signaling hyperactivation. Mol. Cell *52*, 193–205.

Kais, Z., Barsky, S.H., Mathsyaraja, H., Zha, A., Ransburgh, D.J.R., He, G., Pilarski, R.T., Shapiro, C.L., Huang, K., and Parvin, J.D. (2011). KIAA0101 interacts with BRCA1 and regulates centrosome number. Mol. Cancer Res. *9*, 1091–1099.

Kato, T., Daigo, Y., Aragaki, M., Ishikawa, K., Sato, M., and Kaji, M. (2012). Overexpression of KIAA0101 predicts poor prognosis in primary lung cancer patients. Lung Cancer *75*, 110–118.

Kawauchi, D., Robinson, G., Uziel, T., Gibson, P., Rehg, J., Gao, C., Finkelstein, D., Qu, C., Pounds, S., Ellison, D.W., et al. (2012). A mouse model of the most aggressive subgroup of human medulloblastoma. Cancer Cell *21*, 168–180.

Kemper, K., Sprick, M.R., de Bree, M., Scopelliti, A., Vermeulen, L., Hoek, M., Zeilstra, J., Pals, S.T., Mehmet, H., Stassi, G., et al. (2010). The AC133 epitope,

but not the CD133 protein, is lost upon cancer stem cell differentiation. Cancer Res. *70*, 719–729.

Kreso, A., and Dick, J.E. (2014). Evolution of the cancer stem cell model. Cell Stem Cell *14*, 275–291.

Laurenti, E., Varnum-Finney, B., Wilson, A., Ferrero, I., Blanco-Bose, W.E., Ehninger, A., Knoepfler, P.S., Cheng, P.F., MacDonald, H.R., Eisenman, R.N., et al. (2008). Hematopoietic stem cell function and survival depend on c-Myc and N-Myc activity. Cell Stem Cell *3*, 611–624.

Metcalfe, C., Kljavin, N.M., Ybarra, R., and De Sauvage, F.J. (2014). Lgr5+ stem cells are indispensable for radiation-induced intestinal regeneration. Cell Stem Cell *14*, 149–159.

Mizutani, K., Onda, M., Asaka, S., Akaishi, J., Miyamoto, S., Yoshida, A., Nagahama, M., Ito, K., and Emi, M. (2005). Overexpressed in anaplastic thyroid carcinoma-1 (OEATC-1) as a novel gene responsible for anaplastic thyroid carcinoma. Cancer *103*, 1785–1790.

Montgomery, R.K., Carlone, D.L., Richmond, C.A., Farilla, L., Kranendonk, M.E.G., Henderson, D.E., Baffour-Awuah, N.Y., Ambruzs, D.M., Fogli, L.K., Algra, S., et al. (2011). Mouse telomerase reverse transcriptase (mTert) expression marks slowly cycling intestinal stem cells. Proc. Natl. Acad. Sci. USA *108*, 179–184.

Morrison, S.J., and Spradling, A.C. (2008). Stem cells and niches: mechanisms that promote stem cell maintenance throughout life. Cell *132*, 598–611.

Moser, A.R., Pitot, H.C., and Dove, W.F. (1990). A dominant mutation that predisposes to multiple intestinal neoplasia in the mouse. Science *247*, 322–324.

Muñoz, J., Stange, D.E., Schepers, A.G., Van De Wetering, M., Koo, B.K., Itzkovitz, S., Volckmann, R., Kung, K.S., Koster, J., Radulescu, S., et al. (2012). The Lgr5 intestinal stem cell signature: robust expression of proposed quiescent ′+4′ cell markers. EMBO J. *31*, 3079–3091.

Munoz, N.M., Upton, M., Rojas, A., Washington, M.K., Lin, L., Chytil, A., Sozmen, E.G., Madison, B.B., Pozzi, A., Moon, R.T., et al. (2006). Transforming growth factor beta receptor type II inactivation induces the malignant transformation of intestinal neoplasms initiated by Apc mutation. Cancer Res. *66*, 9837–9844.

Nguyen, L.V., Vanner, R., Dirks, P., and Eaves, C.J. (2012). Cancer stem cells: an evolving concept. Nat. Rev. Cancer *12*, 133–143.

Nie, Z., Hu, G., Wei, G., Cui, K., Yamane, A., Resch, W., Wang, R., Green, D.R., Tessarollo, L., Casellas, R., et al. (2012). c-Myc is a universal amplifier of expressed genes in lymphocytes and embryonic stem cells. Cell *151*, 68–79.

O'Brien, C.A., Pollett, A., Gallinger, S., and Dick, J.E. (2007). A human colon cancer cell capable of initiating tumour growth in immunodeficient mice. Nature *445*, 106–110.

Onuma, K., Ochiai, M., Orihashi, K., Takahashi, M., Imai, T., Nakagama, H., and Hippo, Y. (2013). Genetic reconstitution of tumorigenesis in primary intestinal cells. Proc. Natl. Acad. Sci. USA *110*, 11127–11132.

Polakis, P. (2012). Drugging Wnt signalling in cancer. EMBO J. *31*, 2737–2746.

Povlsen, L.K., Beli, P., Wagner, S.A., Poulsen, S.L., Sylvestersen, K.B., Poulsen, J.W., Nielsen, M.L., Bekker-Jensen, S., Mailand, N., and Choudhary, C. (2012). Systems-wide analysis of ubiquitylation dynamics reveals a key role for PAF15 ubiquitylation in DNA-damage bypass. Nat. Cell Biol. *14*, 1089–1098.

Powell, A.E., Wang, Y., Li, Y., Poulin, E.J., Means, A.L., Washington, M.K., Higginbotham, J.N., Juchheim, A., Prasad, N., Levy, S.E., et al. (2012). The pan-ErbB negative regulator Lrig1 is an intestinal stem cell marker that functions as a tumor suppressor. Cell *149*, 146–158.

Ricci-Vitiani, L., Lombardi, D.G., Pilozzi, E., Biffoni, M., Todaro, M., Peschle, C., and De Maria, R. (2007). Identification and expansion of human colon-cancer-initiating cells. Nature *445*, 111–115.

Sangiorgi, E., and Capecchi, M.R. (2008). Bmi1 is expressed in vivo in intestinal stem cells. Nat. Genet. *40*, 915–920.

Sansom, O.J., Meniel, V.S., Muncan, V., Phesse, T.J., Wilkins, J.A., Reed, K.R., Vass, J.K., Athineos, D., Clevers, H., and Clarke, A.R. (2007). Myc deletion rescues Apc deficiency in the small intestine. Nature *446*, 676–679.

Sato, T., Stange, D.E., Ferrante, M., Vries, R.G., Van Es, J.H., Van den Brink, S., Van Houdt, W.J., Pronk, A., Van Gorp, J., Siersema, P.D., et al. (2011a). Long-term expansion of epithelial organoids from human colon, adenoma, adenocarcinoma, and Barrett's epithelium. Gastroenterology *141*, 1762–1772.

Sato, T., Van Es, J.H., Snippert, H.J., Stange, D.E., Vries, R.G., Van Den Born, M., Barker, N., Shroyer, N.F., Van De Wetering, M., and Clevers, H. (2011b). Paneth cells constitute the niche for Lgr5 stem cells in intestinal crypts. Nature *469*, 415–418.

Sato, T., Vries, R.G., Snippert, H.J., van de Wetering, M., Barker, N., Stange, D.E., van Es, J.H., Abo, A., Kujala, P., Peters, P.J., et al. (2009). Single Lgr5 stem cells build crypt-villus structures in vitro without a mesenchymal niche. Nature *459*, 262–265.

Schepers, A.G., Snippert, H.J., Stange, D.E., van den Born, M., van Es, J.H., van de Wetering, M., and Clevers, H. (2012). Lineage tracing reveals Lgr5+ stem cell activity in mouse intestinal adenomas. Science *337*, 730–735.

Sikora, K., Chan, S., Evan, G., Gabra, H., Markham, N., Stewart, J., and Watson, J. (1987). c-myc oncogene expression in colorectal cancer. Cancer *59*, 1289–1295.

Suh, H.N., Kim, M.J., Jung, Y.S., Lien, E.M., Jun, S., and Park, J.I. (2017). Quiescence exit of Tert(+) stem cells by Wnt/beta-Catenin is indispensable for intestinal regeneration. Cell Rep. *21*, 2571–2584.

Takahashi, K., Tanabe, K., Ohnuki, M., Narita, M., Ichisaka, T., Tomoda, K., and Yamanaka, S. (2007). Induction of pluripotent stem cells from adult human fibroblasts by defined factors. Cell *131*, 861–872.

Takaku, K., Oshima, M., Miyoshi, H., Matsui, M., Seldin, M.F., and Taketo, M.M. (1998). Intestinal tumorigenesis in compound mutant mice of both Dpc4 (Smad4) and Apc genes. Cell *92*, 645–656.

Takeda, N., Jain, R., LeBoeuf, M.R., Wang, Q., Lu, M.M., and Epstein, J.A. (2011). Interconversion between intestinal stem cell populations in distinct niches. Science *334*, 1420–1424.

Tetteh, P.W., Basak, O., Farin, H.F., Wiebrands, K., Kretzschmar, K., Begthel, H., Van Den Born, M., Korving, J., De Sauvage, F., Van Es, J.H., et al. (2016). Replacement of lost lgr5-positive stem cells through plasticity of their enterocyte-lineage daughters. Cell Stem Cell *18*, 203–213.

Tian, H., Biehs, B., Warming, S., Leong, K.G., Rangell, L., Klein, O.D., and De Sauvage, F.J. (2011). A reserve stem cell population in small intestine renders Lgr5-positive cells dispensable. Nature *478*, 255–259.

van Es, J.H., Jay, P., Gregorieff, A., van Gijn, M.E., Jonkheer, S., Hatzis, P., Thiele, A., van den Born, M., Begthel, H., Brabletz, T., et al. (2005). Wnt signalling induces maturation of Paneth cells in intestinal crypts. Nat. Cell Biol. *7*, 381–386.

Van Es, J.H., Sato, T., Van De Wetering, M., Lyubimova, A., Yee Nee, A.N., Gregorieff, A., Sasaki, N., Zeinstra, L., Van Den Born, M., Korving, J., et al. (2012). Dll1+ secretory progenitor cells revert to stem cells upon crypt damage. Nat. Cell Biol. *14*, 1099–1104.

Varlakhanova, N.V., Cotterman, R.F., deVries, W.N., Morgan, J., Donahue, L.R., Murray, S., Knowles, B.B., and Knoepfler, P.S. (2010). myc maintains embryonic stem cell pluripotency and self-renewal. Differentiation *80*, 9–19.

Varnat, F., Duquet, A., Malerba, M., Zbinden, M., Mas, C., Gervaz, P., and Ruiz i Altaba, A. (2009). Human colon cancer epithelial cells harbour active HEDGEHOG-GLI signalling that is essential for tumour growth, recurrence, metastasis and stem cell survival and expansion. EMBO Mol. Med. *1*, 338–351.

Wang, H., Yang, H., Shivalila, C.S., Dawlaty, M.M., Cheng, A.W., Zhang, F., and Jaenisch, R. (2013). One-step generation of mice carrying mutations in multiple genes by CRISPR/Cas-mediated genome engineering. Cell *153*, 910–918.

Wang, X., Jung, Y.S., Jun, S., Lee, S., Wang, W., Schneider, A., Sun Oh, Y., Lin, S.H., Park, B.J., Chen, J., et al. (2016). PAF-Wnt signaling-induced cell plasticity is required for maintenance of breast cancer cell stemness. Nat. Commun. *7*, 10633.

Wilson, A., Murphy, M.J., Oskarsson, T., Kaloulis, K., Bettess, M.D., Oser, G.M., Pasche, A.C., Knabenhans, C., Macdonald, H.R., and Trumpp, A.

(2004). c-Myc controls the balance between hematopoietic stem cell self-renewal and differentiation. Genes Dev. *18*, 2747–2763.

Yang, H., Wang, H., Shivalila, C.S., Cheng, A.W., Shi, L., and Jaenisch, R. (2013). One-step generation of mice carrying reporter and conditional alleles by CRISPR/Cas-mediated genome engineering. Cell *154*, 1370–1379.

Yu, P., Huang, B., Shen, M., Lau, C., Chan, E., Michel, J., Xiong, Y., Payan, D.G., and Luo, Y. (2001). p15PAF, a novel PCNA associated factor with increased expression in tumor tissues. Oncogene *20*, 484–489.

Yuan, R.H., Jeng, Y.M., Pan, H.W., Hu, F.C., Lai, P.L., Lee, P.H., and Hsu, H.C. (2007). Overexpression of KIAA0101 predicts high stage, early tumor recurrence, and poor prognosis of hepatocellular carcinoma. Clin. Cancer Res. *13*, 5368–5376.

Zeilstra, J., Joosten, S.P.J., Dokter, M., Verwiel, E., Spaargaren, M., and Pals, S.T. (2008). Deletion of the WNT target and cancer stem cell marker CD44 in Apc(Min/+) mice attenuates intestinal tumorigenesis. Cancer Res. *68*, 3655–3661.

Zhu, L., Gibson, P., Currle, D.S., Tong, Y., Richardson, R.J., Bayazitov, I.T., Poppleton, H., Zakharenko, S., Ellison, D.W., and Gilbertson, R.J. (2009). Prominin 1 marks intestinal stem cells that are susceptible to neoplastic transformation. Nature *457*, 603–607.

STAR★METHODS

KEY RESOURCES TABLE

REAGENT or RESOURCE	SOURCE	IDENTIFIER
Antibodies		
Mouse anti-PAF (KIAA0101)	Santa Cruz Biotechnology	Cat# sc-390515
Mouse anti-PAF (KIAA0101)	Abcam	Cat# ab56773; RRID:AB_943922
Rabbit anti-PCNA	Cell Signaling Technology	Cat# 13110
Rabbit anti-Bmi1	Cell Signaling Technology	Cat# 6964S; RRID:AB_10828713
Rabbit anti-RFP	Rockland	Cat# 600-401-379S; RRID:AB_11182807
Rat anti-BrdU	Abcam	Cat# ab6326; RRID:AB_305426
Rabbit anti-Ki67	Abcam	Cat# ab16667; RRID:AB_302459
Mouse anti-E-Cadherin	BD Biosciences	Cat# 610182; RRID:AB_397581
Rabbit anti-Lysozyme	Abcam	Cat# ab108508; RRID:AB_10861277
Rabbit anti-Villin	Thermo Fisher Scientific	Cat# PA5-22072; RRID:AB_11155190
Rabbit anti-Chromogranin A	Abcam	Cat# ab15160; RRID:AB_301704
Rabbit anti-Phospho-Histone H2A.X (Ser139) (20E3)	Cell Signaling Technology	Cat# 9718S; RRID:AB_2118009
Rabbit anti-Cleaved Caspase-3 (Asp175) (5A1E)	Cell Signaling Technology	Cat# 9664; RRID:AB_2070042
Rabbit anti-β-Catenin (D10A8)	Cell Signaling Technology	Cat# 9587S; RRID:AB_10695312
Rabbit anti-Non-phospho (Active) β-Catenin (D13A1)	Cell Signaling Technology	Cat# 8814S; RRID:AB_11127203
Rabbit anti-c-Myc (N262)	Santa Cruz Biotechnology	Cat# sc-764; RRID:AB_631276
Rabbit anti-Cyclin D1 (92G2)	Cell Signaling Technology	Cat# 2978P; RRID:AB_10839128
Rat anti-CD44	BD Biosciences	Cat# 550538; RRID:AB_393732
Rat anti-CD133	eBioscience	Cat# 14-1331-82; RRID:AB_467471
Mouse anti-P53 (Ab-1)	Thermo Fisher Scientific	Cat# MS-104-P0; RRID:AB_64407
Rabbit anti-P21 (M-19)	Santa Cruz Biotechnology	Cat#sc-471; RRID:AB_632123
Rabbit anti-Phospho-Chk1 (Ser345)	Cell Signaling Technology	Cat#2341; RRID:AB_330023
Mouse anti-ATM pS1981	Rockland	Cat# 200-301-500; RRID:AB_828098
Chemicals, Peptides, and Recombinant Proteins		
5-Bromo-2'-deoxyuridine	Sigma	Cat# B5002
Y-27632 dihydrochloride	Sigma	Cat# Y0503
Recombinant Mouse R-Spondin 1	R&D Systems	Cat# 3474-RS-050
Recombinant Murine Noggin	Peprotech	Cat# 250-38
Recombinant Murine EGF	Peprotech	Cat# 315-09
Jagged-1 peptide	AnaSpec	AS-61298
Critical Commercial Assays		
REPLI-g WTA Single Cell Kit	Qiagen	Cat# 150063

(*Continued on next page*)

Continued

REAGENT or RESOURCE	SOURCE	IDENTIFIER
Experimental Models: Cell Lines		
FHC	ATCC	CRL-1831; RRID:CVCL_3688
HCT116	ATCC	CCL-247; RRID:CVCL_0291
SW620	ATCC	CCL-227; RRID:CVCL_0547
HT29	ATCC	HTB-38; RRID:CVCL_0320
Experimental Models: Organisms/Strains		
Mouse: *Lgr5-EGFP-IRES-creERT2* (B6.129P2-*Lgr5*$^{tm1(cre/ERT2)Cle}$/J)	The Jackson Laboratory	JAX: 008875; RRID:IMSR_JAX:008875
Mouse: *Apc*$^{Min/+}$ (C57BL/6J-*Apc*^{Min}/J)	The Jackson Laboratory	JAX: 002020; RRID:IMSR_JAX:002020
Mouse: *TERT*$^{TCE/+}$	Jun et al., 2016	Jae-il Park, jaeil@mdanderson.org
Mouse: *Bmi1*^{EGFP} (BKa.Cg-*Ptprcb Bmi1*^{tm1Ilw} *Thy1a*/J)	The Jackson Laboratory	JAX: 017351; RRID:IMSR_JAX:017351
Mouse: *C57BL/6J*	The Jackson Laboratory	JAX: 000664; RRID:IMSR_JAX:000664
Recombinant DNA		
MSCV-c-Myc-IRES-RFP	Kawauchi et al., 2012	Addgene #35395
Oligonucleotides		
Primers for qPCR and ChIP, see Table S3	This paper	N/A
Deposited Data		
RNA-seq data set	This paper	GEO: GSE109209

CONTACT FOR REAGENT AND RESOURCE SHARING

Further information and requests for resources and reagents should be directed to and will be fulfilled by the Lead Contact, Jae-Il Park (jaeil@mdanderson.org).

EXPERIMENTAL MODEL AND SUBJECT DETAILS

Mouse Strains

We generated *PAF* KO strain using CRISPR/Cas9 gene targeting system. *Apc*$^{Min/+}$ (JAX: 002020) and *Lgr5-EGFP-IRES-CreERT2* (JAX: 008875) mice were obtained from the Jackson Laboratory. All mice were maintained on a C57BL/6 background except *Bmi1*^{EGFP} mice (BKa.Cg-*Ptprcb Bmi1*^{tm1Ilw}*Thy1a*/J). Both male and female of *PAF KO*, *C57BL/6J* (WT control), or *Lgr5-EGFP* compound strains were used for regeneration experiments in 8-10 weeks of age. For intestinal adenoma quantification and Kaplan-Meier survival curve, only male mice (*Apc*$^{Min/+}$ and *PAF* KO;*Apc*$^{Min/+}$ compound strains) were used. All mouse experiments were performed under MD Anderson guidelines and Association for Assessment and Accreditation of Laboratory Animal Care International standards.

METHOD DETAILS

Generation of *PAF* KO Mice

To establish *PAF* KO mice, two guide RNAs (gRNAs) targeting exon 1 of *PAF* gene and Cas9 mRNA (Sigma) were injected into the mouse zygotes (The Genetically Engineered Mouse Facility, MD Anderson). gRNA sequences were as follows: #1: 5'-GTT CCCGCCACCGTTTAAATGGG-3', #2: 5'-ACCAAAGCAAACTACGTTCCAGG-3'. Four strains harboring *PAF* mutation (gene targeting efficiency: 4/7=57.14%) were identified. Two heterozygote strains (strain 4 and 7) carrying 118bp and 125bp deletion of *PAF* (*PAF null*) between the two gRNAs targeted region were selected as founders. Using the strain 7 as a founder, at least 5 times subsequent backcross with C57BL/6 was conducted to minimize the off-target effects. For PCR genotyping of *PAF* KO following primer pairs and cycling conditions were used: primers: #F: 5' -AGAATCGAGGTTCTCAAGCG-3'; #R: 5'-CCTTCTAGCTGCTCAATGGG-3', PCR

conditions: 10 min at 95°C, followed by 40 cycles of 95°C for 15 sec, 65°C for 15 sec, 72°C for 30 sec and post-elongation at 72°C for 5 min. *PAF* WT makes 280 bp, and *PAF* KO makes 155bp (125bp deletion) of PCR product.

Radiation Injury

For intestinal damage, 8-10 weeks old mice were treated with γ-irradiation (10 or 12 Gy) using irradiator (Nasatron). The intestinal regeneration was assessed at 4 and 7 dpi.

Gene Expression Analysis

For small-scale screening of DNA repair gene expression in mice, mRNAs from the irradiated mouse small intestines (1 dpi, 10 Gy) were analyzed with RT^2 Profiler™ PCR Array Mouse DNA Repair (Qiagen). Control and experimental mice were used for analysis (n=3, each). RNA was extracted from the mouse small intestine and organoids using the TRIzol (Invitrogen) as the manufacturer's instructions. iScript cDNA synthesis kit (Biorad) with 1 μg of RNA was used for cDNA synthesis. For gene expression analysis of Lgr5+ cells, sorted 100-500 Lgr5+ cells were collected from *Lgr5*^{EGFP} or *PAF* KO;*Lgr5-EGFP* mice in normal and IR-treated conditions. cDNA was synthesized using REPLI-g WTA Single Cell Kit (Qiagen #150063). The quantitative real-time PCR (qRT-PCR) was performed using a 7500 real-time PCR machine (Applied Biosystems) with specific primers listed in Table S3. Target gene expression was normalized by Hypoxanthine phosphoribosyltransferase 1 (*HPRT1*) or *18s* rRNA. Comparative $2^{-\Delta\Delta Ct}$ methods were used for quantification of qRT-PCR results.

Crypt Organoid Culture

Crypt organoid culture and *Apc*-mutated organoid culture were performed based on the previous studies (Sato et al., 2009, 2011b). Briefly, the small intestine samples were opened longitudinally and washed with PBS several times. For extracting the crypt, the small intestine was incubated with 5mM EDTA/PBS for 30 min and the crypt-rich supernatant was collected after vigorous shaking. After filtering through the 100 strainers, the same number (300∼500) of crypts were seeded in 50 μl Matrigel (BD). 500 μl of ENR medium (Advanced DMEM/F12 media supplement with EGF (20 ng/ml, Peprotech), Noggin (100 ng/ml, Peprotech) and R-spondin1 (500 ng/ml, Peprotech) were added every two days. For single cell organoid culture, crypts fractions collected through the 70 μm (BD) cell strainer was incubated with Accumax (Stem cell technology 07921) and DNAse (0.8 mg/ml, Sigma) for 30 min. Passaging though the 40 μm strainer, ∼5000 Lgr5^{high} and Cytox Blue (Life technologies) negative cells were collected by cell sorting (MoFlo, Beckman Coulter) and seeded in Matrigel. ENR medium with Jagged-1 peptide (1 μM, AnaSpec) was supplied every 2 days. Organoid efficiency was calculated by counting viable crypts or Lgr5+ cells (at day 3) in total crypts (300∼500 per well, crypt organoid) or total seeded cells (n=∼2000 per well, single cell organoid). For *Apc*$^{Min/+}$ organoids, adenomas were collected and suspended with Advanced DMEM/F12 media supplement with EGF (20 ng/ml) and Noggin (100 ng/ml). Fresh media were supplemented every 3 days until the next passage (10-14 days). Cystic organoid efficiency was calculated by counting viable cells (at day 3) in total suspended cells (Single cell organoid). The size of organoids was analyzed by measuring the area of the middle section of organoids under the microscope using AxioVision software (Zeiss) (at least 30 organoids per group for all experiments).

Organoid Retrovirus Infection

For organoid gene transduction, we utilized the modified method based on the previous reference (Onuma et al., 2013). FACS sorted Lgr5^{high} single cells (n=∼5000) from *PAF* WT and *PAF* KO mice were incubated with media containing retroviruses expressing c-Myc with RFP (MSCV-c-Myc-IRES-RFP, Addgene [#35395]), or wild-type PAF and mutPIP-PAF (Jung et al., 2013) for 6h at 37°C with polybrene (7 μg/ml) and Jagged-1 peptide (1 μM, AnaSpec). Then, infected cells were seeded on 50 μL Matrigel/well in a 12-well plate with conventional ENR media. RFP+ cells were able to observe 2 days after infection. Only RFP+ cells were considered as transfected cells. For selecting nt-PAF or mutPIP-PAF infected organoids, blasticidin (10 μg/ml) was treated.

Lgr5 mRNA Fluorescence In Situ Hybridization (FISH)

WT or *PAF* KO intestinal tissue sections (0 and 7 dpi) were processed for *Lgr5* mRNA FISH according to the manufacturer's protocol (Invitrogen, FISH TagTM RNA Green Kit, with Alexa Fluor® 488 dye). Probe was designed as 530 base pair length targeting the coding sequence of *Lgr5.* A probe for sense strand was used as a negative control.

Mammalian Cell Culture and Sphere Formation Assay

CRC Cell line (HT29) was maintained in DMEM media containing 10% fetal bovine serum. For gene depletion, lentiviruses encoding short hairpins against *PAF mRNA* (MISSION shRNA, Sigma) were stably transduced into target cells and selected using puromycin (2 μg/ml). For counting the CSC population, trypsinized each cell line was counted and incubated with antibodies: CD44v6-APC (1:100, BD-Pharmingen [G44-26]) and CD133-FITC (1: 200, Miltenyi Biotec). Dead cells were excluded by Cytox Blue staining. FACS analysis was performed using FacsJazz Cell Sorter (BD). For sphere formation assay, the limited number of HT-29 cells (5000 cells per ml) were plated in triplicate in the ultra-low attachment plates and grown for six days in serum-free stem cell medium (SCM) supplemented with B27 (Invitrogen), EGF (20 ng/ml, Invitrogen), and bFGF (10 ng/ml, Invitrogen). The number and size of spheres were quantified using AxioVision software (Zeiss).

Chromatin Immunoprecipitation Assay

The mouse small intestines (the duodenum) were minced and cross-linked with 1% formaldehyde for 15 min at room temperature. After quenching by glycine, samples were incubated with lysis buffer (0.5% NP40, HEPES 25 mM, KCl 150 mM, $MgCl_2$ 1.5 mM, 10% glycerol and KOH pH 7.5) containing proteinase inhibitors. Then the nuclear fractions were collected after centrifugation. Cell lysates were subjected to sonication (10 times, 30s on and 30s off, Bioruptor 300 [Diagenode]) with ChIP-lysis buffer (Tris 50 mM pH 8.0, NaCl 150 mM, 0.1% SDS, 0.5% deoxycholate, 1% NP40 and EDTA 1 mM). Supernatant from lysates was used for immunoprecipitation with the primary antibodies. The following antibodies were used for ChIP: RNA Polymerase II (1μg/ml, EMD Millipore [CTD4H8]), mouse-anti PAF (1 μg/ml, Abcam [ab56773]), and normal mouse IgG (1 μg/ml, Invitrogen). ChIP amplicons were detected by ChIP-PCR using the primers listed in STAR Methods.

RNA-sequencing

The total RNA from *Apc*$^{Min/+}$ and *PAF KO;Apc*$^{Min/+}$ adenomas (two biological replicas) were used for RNA-seq. The transcriptome sequencing was performed by BGI (www.bgi.com/global/) with BGISEQ-500. Reads are mapped by Tophat2 and Differential genes are defined by Cuffdiff with $P<0.05$. KEGG analysis was performed by DAVID functional annotation analysis. GSEA analysis is performed with normalized FPKM of all genes with default parameters (Number of permutations=1000, collapse dataset=true, permutation type=phenotype).

QUANTIFICATION AND STATISTICAL ANALYSIS

The Student *t*-test was applied for comparison of two samples. P-values below the 0.05 were considered significantly different. At least three biological and experimental replicas were used for statistical analyses, otherwise described in Figure legends. Error bars represent standard error (S.E.M).

DATA AND SOFTWARE AVAILABILITY

The accession number for RNA-seq data reported in this paper is GEO: GSE109209.

All data is available upon request.